2019

DETERMINATION OF ACOUSTIC RADIATION EFFICIENCY VIA PARTICLE VELOCITY SENSOR WITH APPLICATIONS

Steven Conner Campbell
University of Kentucky, scconner95@gmail.com
Digital Object Identifier: https://doi.org/10.13023/etd.2019.119

DETERMINATION OF ACOUSTIC RADIATION EFFICIENCY VIA PARTICLE
VELOCITY SENSOR WITH APPLICATIONS

_____

THESIS

_____

A thesis submitted in partial fulfillment of the
requirements for the degree of Master of Science
in Mechanical Engineering in the College of Engineering
at the University of Kentucky

By

Steven Conner Campbell

Lexington, Kentucky

Director: Dr. David W. Herrin, Professor of Mechanical Engineering

Lexington, Kentucky

2019

ABSTRACT OF THESIS

DETERMINATION OF ACOUSTIC RADIATION EFFICIENCY VIA PARTICLE
VELOCITY SENSOR WITH APPLICATIONS

Acoustic radiation efficiency is defined as the ratio of sound power radiated to the surface vibration power of a piston with equivalent surface area. It has been shown that the radiation efficiency is maximized and may exceed unity when the structural and acoustic wavelengths are approximately equal. The frequency at which this occurs is called the critical frequency and can be shifted with structural modifications. This has proven to be an effective way to reduce noise. The standard radiation efficiency measurement is comprised of an intensity scan for sound power measurement and accelerometer array for spatially averaged vibration determination. This method is difficult to apply to lightweight structures, complicated geometries, and when acoustic sources are in close proximity to one another. Recently, robust particle velocity sensors have been developed. Combined with a small microphone in the same instrument, particle velocity and sound pressure can be measured simultaneously and at the same location. This permits radiation efficiency to be measured using a non-contact approach with a single sensor. A suggested practice for measuring radiation efficiency has been developed and validated with several examples including two flat plates of different thickness, an oil pan, and components on a running small engine.

KEYWORDS: acoustic radiation efficiency, PU probe, particle velocity, coincidence frequency

Steven Conner Campbell

April 22, 2019

DETERMINATION OF ACOUSTIC RADIATION EFFICIENCY VIA PARTICLE
VELOCITY SENSOR WITH APPLICATIONS

By

Steven Conner Campbell

Dr. D. W. Herrin

Director of Thesis

Dr. Alexandre Martin

Director of Graduate Studies

April 22, 2019

Date

ACKNOWLEDGEMENTS

TABLE OF CONTENTS

LIST OF FIGURES

CHAPTER 1 INTRODUCTION

Noise control engineers strive to reduce the sound radiated from machinery in an effort to manufacture a product that is quieter. This in turn allows a company to vend a product that is not only quieter but also safer and more marketable. Machinery noise primarily results from combustion or mechanical mechanisms (piston slap, gear impact, etc.) producing high forces. These harmonic forces produce structural vibration which in turn vibrates the air next to the structure. These airborne vibrations propagate away from the structure and produce what is commonly referred to as noise. It follows that machinery noise can attenuated by 1) reducing the forces which produce the vibration, 2) reducing the vibration by making modifications to the structure, 3) by blocking the path from machinery to receiver using barriers, or 4) reducing how efficiently the structure radiates noise.

Structural vibration is the direct result of the forces acting on a structure. By reducing internal forces, vibration can be reduced by a proportional amount. This is accomplished by two main methods; controlling operating conditions and changing mechanical design. Operating conditions of mechanical equipment include firing frequency, crank angle, engine speed, etc. While these operating conditions are normally optimized to improve performance, they can also be adjusted to reduce noise. Noise reduction in this case is accomplished by controlling operating conditions to lower the dynamic force amplitudes on the structure or avoid exciting resonant frequencies of the system. Resonance occurs at natural frequencies where systems have high vibrational amplitudes even if dynamic forces are low. These frequencies are primarily determined by the mass and stiffness of the structure.

At a resonant frequency, vibration amplitude is high. Avoiding input force harmonics that correspond with these frequencies, reduces the total force experienced by the structure, in turn reducing noise. For example, if a single-cylinder engine has an operating speed of 3600 RPM this corresponds to a 60 Hz engine order. If the engine design has a resonance at this 60 Hz frequency, high vibration amplitude will be likely. By adjusting the operating speed or structure, engine harmonics will no longer correspond to natural

frequencies of the structure and a significant noise reduction may be achieved at the harmonic frequencies of the inputs.

Controlling internal forces and operating conditions is not the only way to reduce radiated noise. Noise can also be attenuated by making structural modifications that change system mechanical properties. By changing mass and stiffness, system resonances can be avoided by shifting natural frequencies higher and lower in frequency. Natural frequencies are moved higher in frequency if the stiffness is increased or the mass is decreased. The converse occurs if stiffness is decreased and mass increased. Stiffness is most commonly increased by adding ribs or increasing thickness. While mass and stiffness directly affect the frequencies at which resonance occurs, damping reduces the amplitude of vibration at the system natural frequencies. Damping is increased by adding constrained layer damping treatments or may be introduced at attachment points between components.

Alternatively, changes can be made to the acoustic path by adding obstructions between the source and receiver. This is done by understanding the path that noise propagates as it travels from the source to the receiver. By shielding an operator from noise via barriers, partitions or enclosures, the sound propagation path is altered, interrupting the generated sound. These treatments work best when the receiver point is completely enclosed from the acoustic source or treatments are placed in areas that offer maximum attenuation. These treatments offer various benefits and are quite effective, but in many cases are large and expensive to construct.

A less obvious approach to reduce the radiated noise is to attempt to reduce how effectively the structure radiates noise. Radiated sound is highly dependent on material and geometric properties of a structure. When an excited structure is vibrating at a structural wavelength much lower than the acoustic wavelength, there is cancellation of sound at the surface.

Radiation efficiency is a measure used to characterize how effectively a structure radiates noise. Radiation efficiency is low at low frequencies then sharply rises when the

structural and acoustic wavelengths are similar in length. This frequency is commonly referred to as the coincidence frequency (f_c).

Noise can sometimes be controlled by shifting the coincidence frequency higher in frequency and away from operating frequencies and their first several harmonics. This is normally accomplished by increasing the compliance of the structure. However, this must be done with care because increasing compliance necessarily entails an increase in the vibration amplitude. In addition, this approach normally cannot be applied on a load bearing structure without adversely affecting the durability. Adding damping to a structure changes the amplitude of vibration but does not affect radiation efficiency. On the other hand, the locations of the input forces may affect radiation efficiency since the deformation shape is affected.

Radiation efficiency can be determined using a combination of structural finite element analysis and acoustic boundary or finite element analysis prior to prototyping. After prototyping, radiation efficiency can be measured. Direct measurement is sometime advantageous because simulation depends on having correct material properties, boundary conditions at connections, and input forces. Experimental methods also reduce the amount of time needed to determine radiation efficiency and find the coincidence frequency of the system. Simulation for radiation efficiency depends on having adequate structural and acoustic models that are coupled with one another correctly. Describing the correct forcing functions of a complex structure can also be incredibly difficult in simulation without adequate knowledge of the vibratory dynamic excitations. Once the coincidence frequency is obtained, structural modifications can be performed, and changes can be observed via performing the experiment again or using a simulation to correlate the change.

Current methods for determining radiation efficiency experimentally utilize two main experiments; a vibratory test for surface velocity determination and an acoustic test for radiated sound power. This two-part method requires a combination of multiple acoustic and vibration sensors. Normally, a large number of sensors and channels are required to

expedite the measurement. However, accelerometers can mass load the structure corrupting the measurement.

Recently, robust particle velocity probes have been developed that accurately measure particle velocity. They are small and can be positioned close to a measurement surface. They have the advantage of being highly directional. The particle velocity sensor has been combined with a small hearing aid microphone. The combination sound pressure and particle velocity sensor is referred to as a PU probe. By measuring particle velocity and sound pressure simultaneously, sound power can be measured and surface vibration can be approximately measured since the sensor is small and can be positioned next to the vibrating source. The advantages of the PU probe are several. 1) It is a non-contact sensor so the modal character of the structure is not changed due to mass loading of the sensor. 2) Sound intensity measurements with the combination sound pressure and particle velocity probe are extremely directional and are accurate in a sound field with nearby sources. 3) Radiation efficiency can be determined for separate components along with the entire structure. 4) Both quantities needed for a radiation efficiency calculation can be measured (sound power and vibration) simultaneously.

The objective of this research is to develop protocol for measuring radiation efficiency with the combination sound pressure and particle velocity sensor or PU probe. Measurement with the PU probe is compared against traditional measurement approaches. A possible protocol is developed and tested on several examples. The objectives of the research are as follows.

Objectives:

1. Test the accuracy of the PU probe for measurement of surface velocity by comparing it to accelerometer measurements.
2. Test the accuracy of the PU probe for measuring sound intensity by comparing to the sound intensity scanning approach
3. Test the accuracy for measuring radiation efficiency with the PU probe by comparing to the standard approach defined in ISO-7849 [1].
4. Develop a protocol for determining radiation efficiency with the PU probe.

5. Develop a simple protocol for accurately adjusting a particle velocity measurement at some distance away from a source to the actual surface velocity.
6. Qualify the method by comparing results on four different structures of varying shape, thickness, and material.
7. Draw several conclusions and suggest future research.

An outline for the remainder of this work is as follows. Chapter 2 provides a literature review of past work on both radiation efficiency and the PU probe. Chapter 3 details the experimental methods utilized to determine radiation efficiency on various geometries along with an initial comparison between measurement techniques. Chapter 4 offers a discussion on correcting velocity measurements with the PU probe and a final analysis of radiation efficiency results. Chapter 5 offers suggestions for future research, outlines the importance of this work, and concisely summarizes the key takeaways from previous chapters.

CHAPTER 2 BACKGROUND AND LITERATURE REVIEW

2.1 Radiation Efficiency Equation

Radiation efficiency for a structure is defined as the ratio between the radiated sound power and the equivalent power of a baffled piston with the same surface area and spatially average vibratory response [2]. Acoustic radiation efficiency is defined as

$$\sigma_{rad} = \frac{W}{\rho c S_{tot} \bar{v}^2} \tag{2.1}$$

where W is the airborne sound power emitted by the structure, $\bar{v}^2$ is the spatially averaged RMS value of velocity across the surface, S_{tot} is the total surface area, ρ is the mass density of fluid, and c is the speed of sound [3]. A piston in a baffle is a very efficient sound radiator and is very much like a loudspeaker. Moreover, the sound power is easily calculated using the simple expression in the denominator of Equation 2.1. However, a piston is not the most efficient radiator and thus radiation efficiency may sometimes exceed 1.

The radiation efficiency of flat panels (plates) [4-7] is well understood. Panels radiate sound effectively whenever the acoustic wavelength is similar in length to or shorter than the structural wavelength. The acoustic wavelength is defined as

$$\lambda_a = \frac{c}{f} \tag{2.2}$$

where c is the speed of sound and f is frequency, With this relationship, acoustic wavelength is proportional to $1/f$ [8]. The bending stiffness of a thin plate can be defined as

6

$$B = \frac{Eh^3}{(12[1 - v^2])} \tag{2.3}$$

where E is Young's modulus, v is Poisson's ratio, and h is thickness of the panel. The panel bending wave speed, c_p , is given as

$$c_p = \left(\frac{B\omega^2}{\rho_m h}\right)^{\frac{1}{4}} \tag{2.4}$$

where ω is angular frequency, h is plate thickness, and ρ_m is the panel surface density [9]. This implies that for a bending plate, the structural wavelength (λ_p) is proportional to $1/\sqrt{f}$.

 For low frequencies, $\lambda_p \ll \lambda_a$, the acoustical wavelength will always be larger than the structural wavelength and the panel bending waves produce positive and negative sources which cancel one another out. Radiation efficiency is low at these frequencies. At high frequencies, ($\lambda_p \gg \lambda_a$), there is little cancellation and the radiating plate acts like a set of uncorrelated point sources.

Radiation efficiency increases sharply when the structural and acoustic wavelengths are nearly equal in length. This frequency is commonly referred to as the coincidence frequency (f_c). At this frequency, acoustic and flexural waves have the same wave speed and wave length causing sound radiation to increase. Figure 2.1 denotes this phenomenon for various flat plates on a log scale. Notice that as frequency increases to the coincidence frequency, radiation efficiency is maximized. By varying the plate panel perimeter, P, surface area S, and thickness h, radiation efficiency at frequencies below the coincidence frequency can be adjusted.
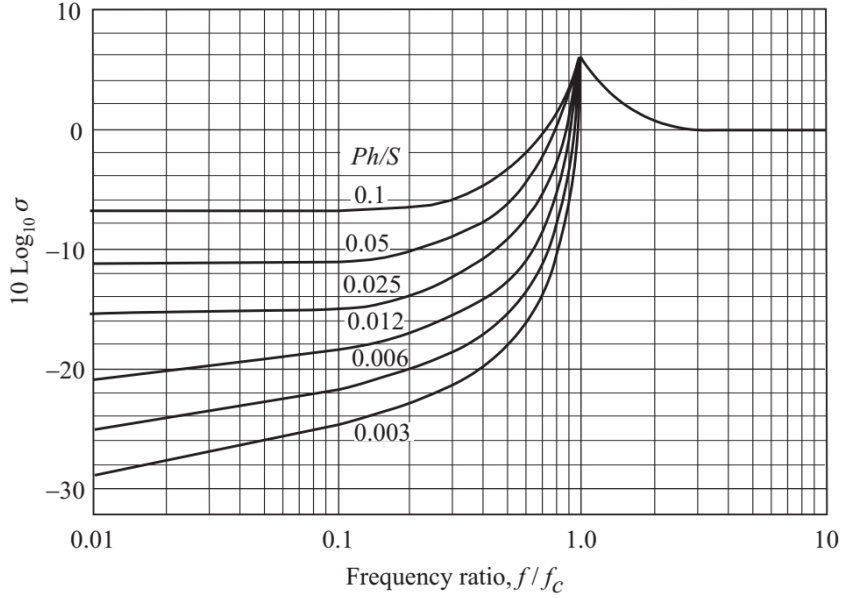
Figure 2.1 – Radiation efficiency as a function of frequency for plates of varying dimensions [10].

Coincidence frequency is a function of the material properties, plate thickness, and the speed of sound of the gas. Combining Equations 2.2 and 2.4, coincidence frequency can be expressed as

$$f_c = \frac{c^2}{2\pi} \sqrt{\frac{12(1-v^2)\rho_s}{Eh^3}} \qquad (2.5)$$

where E is the elastic modulus of the plate, ρ_s is the surface density in units of mass per unit area, v is the Poisson's ratio of the plate, and h is plate thickness [11]. From Equation 2.5, it is evident that coincidence frequency is not dependent on force amplitude. Rather, coincidence frequency can be altered by modifying the material properties and especially thickness of the plate. If the stiffness is increased strategically by adding ribs, the coincidence frequency will increase. Conversely, the coincidence frequency will be reduced if mass is added carefully. That being said, the most effective

method for changing the coincidence frequency is to change the thickness of a panel. The bending stiffness of a panel is proportional to the thickness cubed whereas mass is proportional to thickness. Damping, on the other hand, only has a small effect on coincidence frequencies and radiation efficiency. It reduces the vibration amplitude and the resulting sound power from a time-varying force [12], but radiation efficiency is unchanged.

Consideration of radiation efficiency has been proven beneficial in designing gearbox and drivetrain housings [13-14], and engine components like oil pans [15]. Intuitively, stiffening a structure will result in less sound radiation. However, it is sometimes better to reduce stiffness so that the coincidence frequency will be above the major source harmonics. Load bearing structures like engine blocks or supercharger housings must be stiff for durability reasons. However, non-load bearing structures like oil pans and some housings may be thin or more compliant. The structure can then be designed to maximize the coincidence frequency while still making sure that durability requirements are met.

Another interesting application of radiation efficiency is the design of an acoustic guitar. In contrast to the previous case, musical instruments need to radiate sound in a certain way or level to meet sound quality expectations. By understanding how geometry, material properties, and bracing affects the radiation efficiency of a guitar, a manufacturer can produce a more desirable product. Comparisons between the radiation efficiency of various acoustic guitars have been made in literature [16].

The procedure for determining radiation efficiency in a simulation model is straightforward. Structural finite element analysis is first performed to determine the structural vibration. This analysis is predicated on knowing input forces, damping, and assigning representative boundary conditions. The structural analysis is followed by acoustic finite or boundary element analysis to determine the radiated sound power [14,17,18]. Once sound power and structural vibration are known, radiation efficiency is readily calculated for the system as a whole or individual panels.

Though the analysis process is straightforward, input forces are often not known until a prototype has been manufactured and operated. Moreover, connections at bolt locations

are difficult to model realistically. Moreover, thin components like shields and valve covers deform when they are bolted or riveted changing the structural properties. Hence, it is sometimes simpler to measure radiation efficiency after the component prototype has been manufactured. The main advantages are that the machinery can be running under normal operating conditions and no simplifications are made for simulation purposes.

Measurement of radiation efficiency is a two-step process. From Equation 2.1, it can be seen that acoustic sound power and average surface velocity must be determined. A standard procedure for conducting the experiment is provided in ISO-7849 [19]. 1) The vibration on the surface of the machine is measured using accelerometers. 2) The radiated sound power is measured at a distance away from the source using a sound intensity scan. The test is illustrated in Figure 2.2.
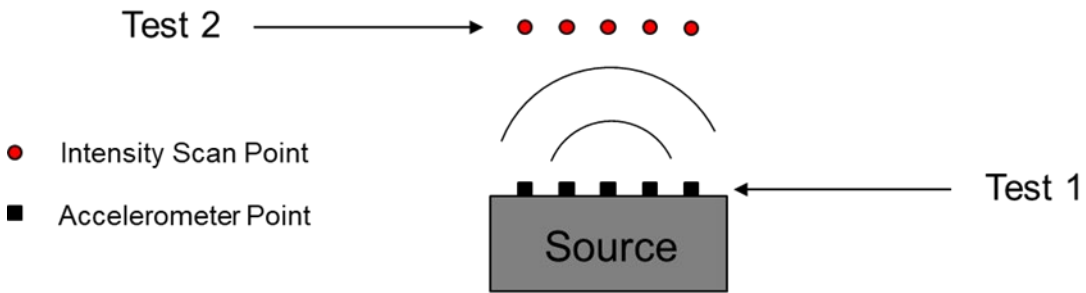
Figure 2.2 – Radiation efficiency experiments according to ISO-7849.

2.2 Surface Velocity Determination

The most common method of measuring the surface velocity is to attach several accelerometers to the vibrating structure. The velocity amplitude (v_j) is determined using

$$v_j = \frac{a_j}{2\pi f} \tag{2.6}$$

where a_j is the acceleration amplitude and f is the frequency in Hz. The spatially averaged vibration for a non-uniformly distributed sensor array can be expressed as

$$\bar{v} = \frac{1}{S_{tot}} \sum_{j=1}^{K} S_j \frac{a_j}{2\pi f} \qquad (2.7)$$

where K is the number of measurements and S_j is the surface area of each patch. One disadvantage of using accelerometers is that they can mass load a structure modifying its modal frequencies. This is especially the case for panels including thin plastic engine covers, some oil pans, and acoustic guitars.

2.3 Sound Power Determination

Sound power must be measured to obtain the numerator in Equation 2.1. One method that is commonly used to determine the sound power radiated is the sound intensity scan. The sound intensity can be averaged over a surface by roving the probe and taking care to evenly sample the sound intensity over a surface. Sound intensity can also be sampled at individual points though the former approach is normally used. The sound intensity is expressed as

$$\bar{I}_n = Re\langle \tilde{P}, \tilde{U}_n^* \rangle \qquad (2.8)$$

with $\tilde{P}$ is the sound pressure and $\tilde{U}_n^*$ is the complex conjugate of particle velocity [20, 21]. Due to difficulty in measuring particle velocity directly, the sound intensity is normally determined using two closely space microphones. The particle velocity can be measured accurately parallel to the microphones. The sound intensity is expressed as

$$\bar{I}_n = \frac{|\tilde{P}_1 \tilde{P}_2|}{\omega \rho_o d} \sin(\varphi_1 - \varphi_2) \qquad (2.9)$$

where d is the separation distance and the difference between φ_1 and φ_2 is the phase difference between microphones [22, 23]. In order for the measurement to be accurate, the two microphones must be phase calibrated with respect to one another. Normally, the sound intensity is scanned over a surface. To determine the total sound power through a scanned surface, the sound intensity is multiplied by the surface area of the surface scanned. If N surfaces surround a source, the sound power can be expressed as the sum of the N sound powers [24]. This is expressed as

$$W = \int_S \bar{I}_n dS \approx \sum_{i=1}^{N} \bar{I}_n \Delta S_i \qquad (2.10)$$

where S_i is the surface area for each patch.

The protocol for measurement of sound intensity scanning is provided in ISO-9614-2 [25]. The proper protocol for the method has been discussed in the literature [26-28]. It is especially noteworthy that maximum frequency for accurate measurement is a function of the separation distance between the two microphones. In addition, the microphones must be phase matched or a phase calibration step must be performed prior to measurement. The method is prone to problems if there is a strong source in a direction transverse to the line formed by the two microphones as illustrated in Figure 2.3. In that case, the phase difference between microphones is difficult to measure accurately due to signal to noise issues.
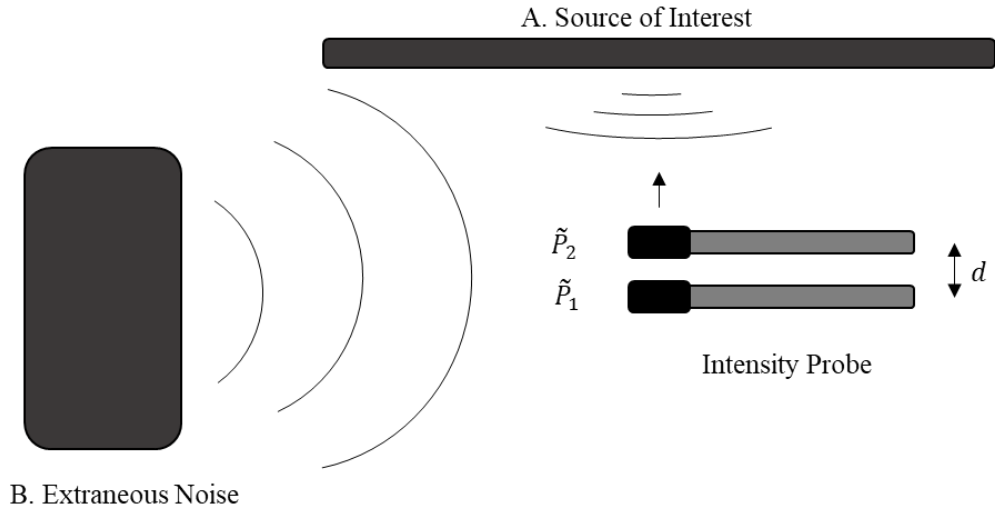
Figure 2.3 – Signal to noise issue with traditional two-mic intensity probe. If Source B is much stronger than Source A, intensity measured in the direction of interest is "drown out".

2.4 The Microflown PU Probe

Acoustic particle velocity is one of two quantities needed to determine sound power of an acoustic disturbance (the other being sound pressure). Particle velocity is defined as the volume flow divided by the fluid surface in which the acoustic wave propagates [29]. Historically, acoustic particle velocity is difficult to measure and was not directly measured until recently, unlike sound pressure which is easily obtainable with microphones.

Particle velocity can now be measured directly with the advent of particle velocity sensors [30]. The Microflown PU probe, in particular, is commercially available after extensive development work. The PU probe consists of two main elements – a Microflown (particle velocity sensor) for measuring particle velocity and a microphone for sound pressure. The Microflown or µ-sensor is made of two thin closely spaced wires with a conductive metal covering over them [31]. This sensor directly measures particle velocity. This is accomplished by use of thermal principles [32, 33].

13
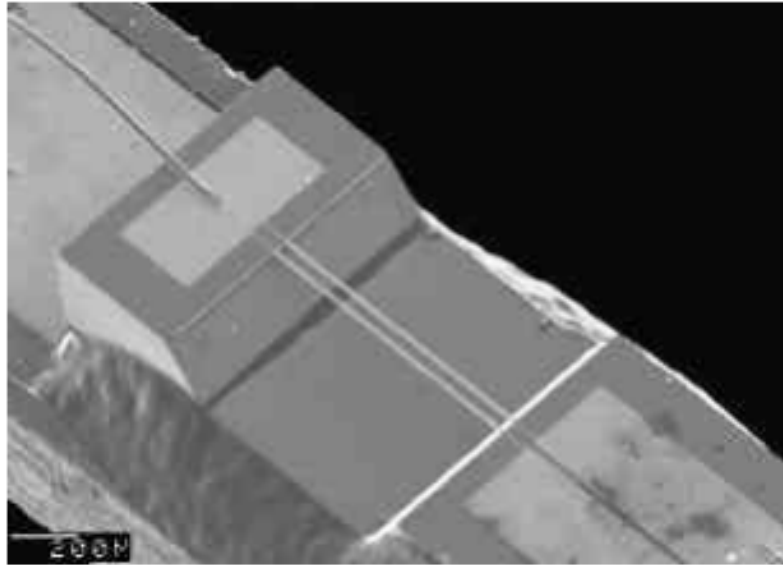
Figure 2.4 – Microflown PU probe μ-sensor design. Two hot wires separated by a small spacing. As current is placed across the bridge, the wires heat up [35].

By applying a voltage across the metal conductor, the parallel wires heat up. By measuring the temperature difference between the wires, particle velocity can be determined [34]. This is very much like a hot wire anemometer sensor. Figure 2.4 shows a typical Microflown design [35]. During operation, the two parallel wires are heated up to above 200°C [36]. As air oscillates across the bridge, one wire is cooled more than the other [37]. This is dependent on the direction of the particle velocity [38]. By utilizing temperatures sensors to measure both positive and negative temperature drops across the wires, particle velocity amplitude can be measured [39]. Since the direction of air motion produces a temperature change across the wires in a specific direction, the probe is directional. A schematic of the sensor is shown in Figure 2.5.

With the Microflown and a miniature microphone both integrated into the same packaging, the PU probe has the capability to measure sound intensity directly [41]. Accurate measurement of sound intensity with this probe relies on proper calibration of both the particle velocity sensor and microphone in the PU probe.
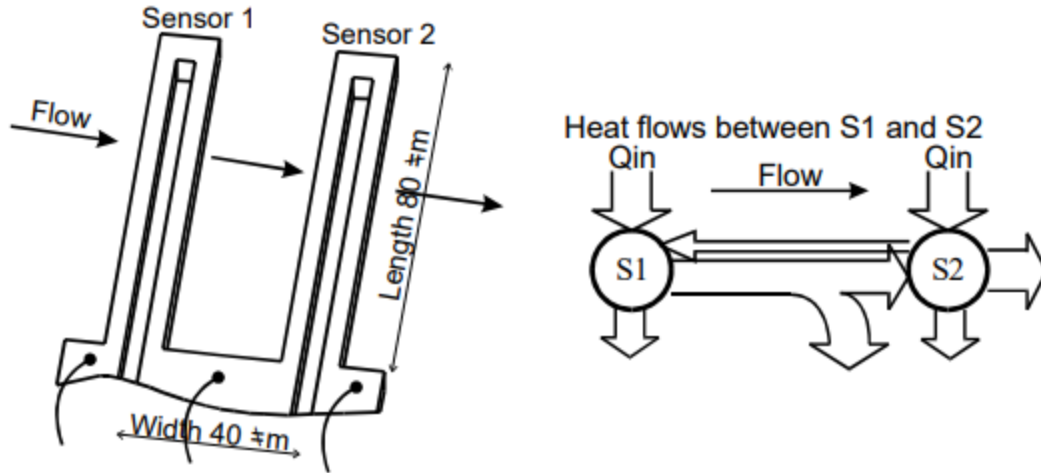
Figure 2.5 – Microflown thermal mechanics. As air flows across S1 and S2, a temperature drop causes a differential electrical resistance variation [40].

Particle velocity is most easily calibrated by utilizing the relationship between particle velocity and sound pressure in the far field. If a loudspeaker is placed on the floor of an anechoic chamber, a microphone and particle velocity sensor can be located at a specified distance away from the loudspeaker as shown in Figure 2.6. Assuming the loudspeaker acts as a monopole, particle velocity can be expressed as

$$u(r) = \frac{p(r)}{\rho c} \times \left(1 + \frac{1}{jkr}\right) \qquad (2.11)$$

where r is the distance from the source, c is the speed of sound, rho is the density, and k is the acoustic wavenumber [42]. Acoustic wavenumber can be expressed as

$$k = \frac{\omega}{c} \qquad (2.12)$$

15

where omega is the angular frequency and c is the speed of sound. Note that the second term on the right-hand side becomes unimportant as kr becomes large.
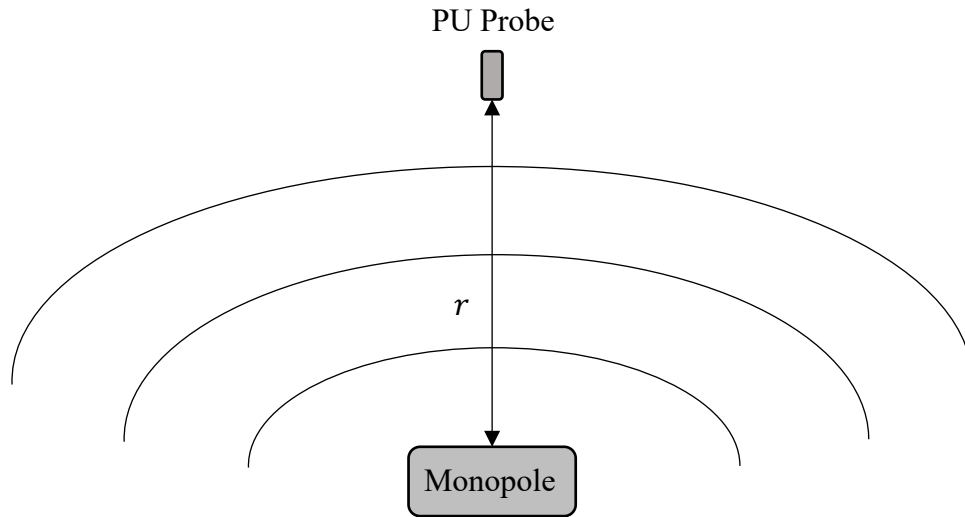
Figure 2.6 – Test setup for PU probe calibration in an anechoic chamber.

The particle velocity sensor can also be calibrated in an impedance tube so long as plane wave propagation can be assumed. A schematic of the test setup is shown in Figure 2.7. By placing the PU probe at a point x in a closed tube with length l and driving the air with a loudspeaker, particle velocity can be related to sound pressure as [43- 44]

$$u(x) = p(x) \times \frac{j}{\rho c} \tan(k(l - x)) \tag{2.13}$$

This method requires the probe to be carefully positioned in the impedance tube. The interface between the probe and tube must be well sealed or the measurement will be compromised.
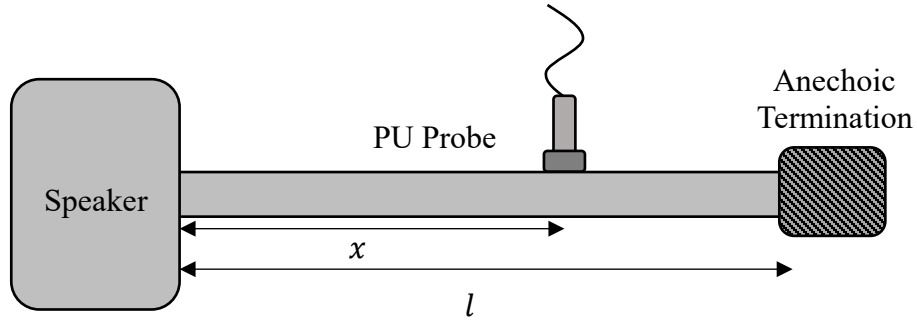
Figure 2.7 – Test setup for PU probe calibration in impedance tube.

It is noteworthy that the particle velocity sensor is not able to measure the surface vibration directly. Particle velocity rapidly decays as the distance from a source is increased. Very close to a source, the particle velocity and surface vibration are similar [45]. Ref. [46-48] explore the accuracy of using the particle velocity sensor to measure surface vibration if the sensor is positioned close to the surface.

For an ideal case of a circular piston in a baffle, the particle velocity can be expressed as a function of distance (x) and piston radius (a) [49]. The particle velocity complex amplitude can be expressed as

$$u_n(x) = v_n\left(1 - \beta e^{-2i\gamma}\right) \tag{2.14}$$

with

$$\beta = \frac{x}{\sqrt{x^2 + a^2}} \tag{2.15}$$

and

$$\gamma = k\left(\frac{\sqrt{x^2 + a^2} - x}{2}\right) \tag{2.16}$$

where k is the acoustic wavenumber defined as the angular frequency divided by the speed of sound. If Equation 2.14 is solved for the surface vibration and simplified, the expression

$$v_n(x) \approx \frac{u_n(x)}{(\beta^2 - 2\beta \cos 2\gamma + 1)} \qquad (2.17)$$

is obtained. In Equation 2.17, note that the surface and particle vibration are only equal to each other if β is very small. In order for particle velocity to approximate the surface velocity, the probe will need to be as close the surface as possible. Note that the relationship between surface vibration and particle velocity is also a function of frequency since gamma is a non-dimensional frequency term. Though a relationship between surface vibration and particle velocity can be obtained for the ideal case of a baffled piston, an equation relating the two cannot be developed for the general case.

The PU probe can also be used to measure the sound intensity which is normally measured using a two-microphone approach. The measurement protocol for determining sound intensity using a two-microphone approach is detailed in ISO-9614-2 [25]. The accuracy of the PU probe when compared to a two-microphone probe has been explored in detail and is an accurate alternative intensity probe with similar measurement accuracy [50-51]. In some cases, the increased directionality of the PU probe leads to more accurate results than the two-microphone method, especially when various sources are present and in strongly reactive near fields [52]. The two-microphone method is also very sensitive to errors with phase mismatching between the two microphones used in the probe [53]. The PU probe on the other hand, is not as sensitive to these phasing errors between the velocity sensor and microphone.

The PU probe has been used in many applications ranging from assessing engine noise to functioning as a battlefield acoustics sensor [54-58]. The application of the PU probe to radiation efficiency has been explored minimally. Functioning as both a velocity sensor and intensity probe, the PU probe can determine both fundamental quantities needed to determine radiation efficiency. Utilizing these capabilities, the PU probe is proposed to

simplify measurement of radiation efficiency by measuring both particle velocity and sound intensity.

CHAPTER 3 EXPERIMENTAL METHODS

3.1 Introduction to Experimental Methods

As expanded upon in Chapter 2, determination of radiation efficiency consists of two separate measurements of radiated sound power and surface vibration. Sound power is traditionally measured with a sound intensity scan that utilizes a two-microphone probe and surface vibration is measured with an accelerometer array. The Microflown PU probe has been proposed as a replacement since both particle velocity and sound pressure can be measured simultaneously. Since both quantities are measured, the PU probe can be used to measure sound intensity. The PU probe may also be used to estimate surface vibration since it can measure particle velocity near a vibrating source.

Four separate test structures were selected for radiation efficiency measurements using the standard approach and the PU probe. These consisted of the following: 1) a flat aluminum plate, 2) a flat stainless-steel plate, 3) a ribbed, aluminum oil pan, and 4) a gas tank connected to a single cylinder engine. These structures were chosen to achieve a wide variety of geometries, materials, and applications. The flat plates are simple geometries that are easily understood in literature. On the other hand, the oil pan and gas tank are much more complex in shape and radiation efficiency is more difficult to determine with simulation or analytical approaches. This selection includes several types of sound radiating structures that represent those found commonly in machinery.

By utilizing methods described in ISO-7849, radiation efficiency was measured for each of the test cases above. This was accomplished by first measuring the sound power radiated off the surface of the structure with the PU probe. After power was determined, accelerometers were attached to the structure and average surface velocity was obtained The PU probe was then moved closer to the vibrating surface, and particle velocity was measured directly above accelerometer locations. This distance away from the surface was minimized to reduce the error between the PU probe and the accelerometers. Radiation efficiency was then calculated for the standard method and the PU probe via Equation 2.1. For this work, Siemens LMS Test.Lab software and a Siemens SCADAS 8 channel data acquisition (DAQ) system were used to record time data.

3.2 PU Probe Calibration

3.2.1 Sound Pressure Calibration

The probe was calibrated in the chamber at the University of Kentucky. Calibration was undertaken according to the method described in Section 2.4. By placing a loud speaker in the center of the anechoic chamber and the PU probe at a distance of 1.8 meter away from the source, sound pressure and particle velocity can be calibrated to microphone measurements. Since the speaker can be assumed to be a monopole source at this distance, particle velocity and sound pressure can be related with Equation 2.11 from Section 2.4 and is shown below.

$$u(r) = \frac{p(r)}{\rho c} \times \left(1 + \frac{1}{jkr}\right) \tag{3.1}$$

Through placing a quarter inch microphone directly next to the PU probe, sound pressure can be calibrated simply. First the loudspeaker was excited with white noise from 0-10000 Hz. Sound pressure was measured at 1.8 meters away from the center of the speaker with the PU probe and quarter inch microphone simultaneously. The sensitivity amplitude of the microphone in the PU probe was then determined by dividing the raw voltage measured by the PU probe's microphone by the pressure measured by the quarter inch microphone. Phase was also measured between the two microphones. Sensitivity results for the microphone in the PU probe are detailed in Figure 3.1 and 3.2.

Measurements were compared to sensitivity curves provided by the manufacturer. There are noticeable differences at very low frequencies, but this is outside the frequency range of interest. Differences at low frequencies can be ignored for the purpose of this work. It was decided to use the calibration curves from the manufacturer though the measured calibrations could be used as well.

21
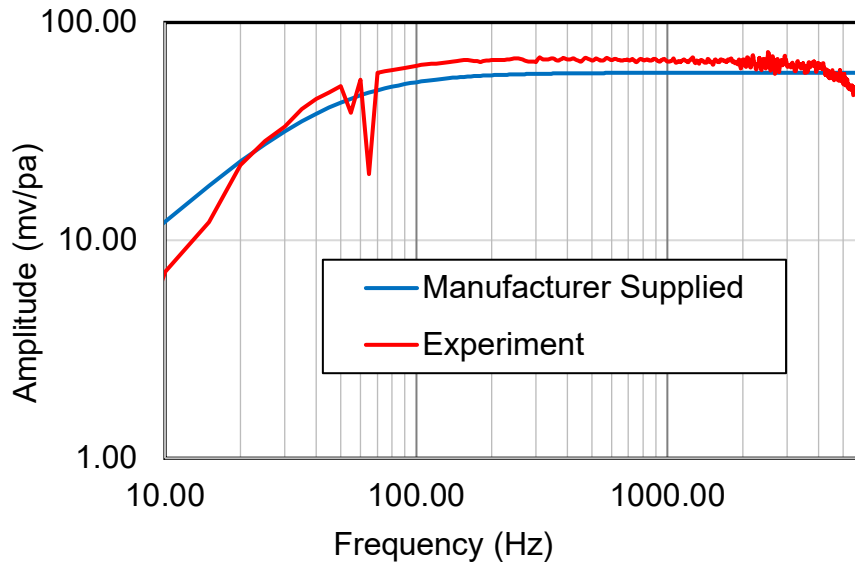
Figure 3.1 – Measured sound pressure sensitivity of the microphone in the PU probe, 0-10000 Hz.
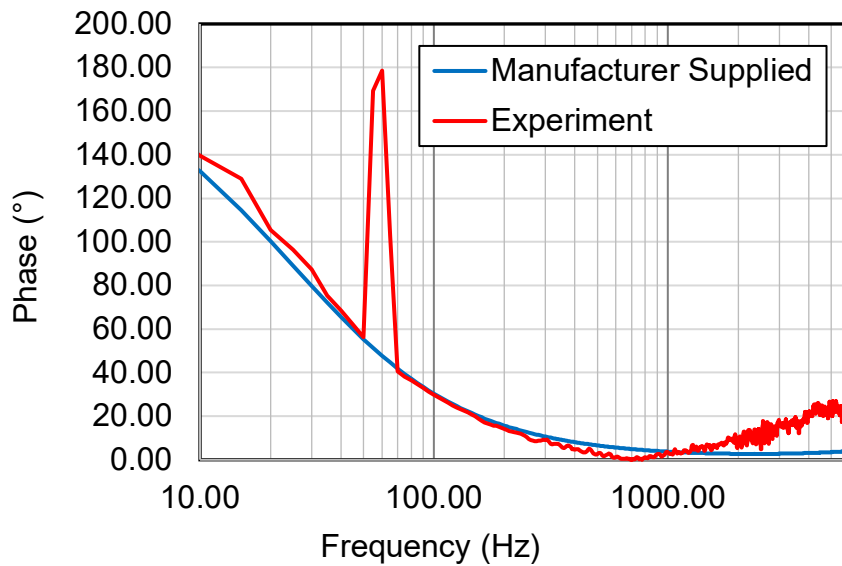
Figure 3.2 – Measured phase difference between of the microphone in the PU probe and a quarter inch microphone, 0-10000 Hz.

3.2.2 Particle Velocity Calibration

Similar to the sound pressure calibration, particle velocity was calibrated for the PU probe. While the sound pressure is a straightforward comparison to a quarter inch microphone, particle velocity must be derived from the sound pressure assuming a monopole source. By assuming that at 1.8 meter away from the presumed monopole source, near field effects can be ignored and the particle velocity can be expressed as a function of sound pressure using Equation 3.1. Particle velocity calibration results are compared to analytical curves from the manufacturer in Figure 3.3 and 3.4.

Also, the sensitivity of the velocity sensor in the PU probe is lower than the expected values from the manufacturer in low frequency ranges. The loudspeaker with white noise excitation could not supply enough power at low frequencies. In addition, the hemi-anechoic chamber itself is only qualified down to 150 Hz. It was elected to use the manufacturer's calibration for particle velocity as before though the measured value could also be used. The manufacturer's calibration is selected because the loudspeaker used does not provide enough power at low frequencies and is not a perfect point source, and there will be some diffraction effect at the microphone.
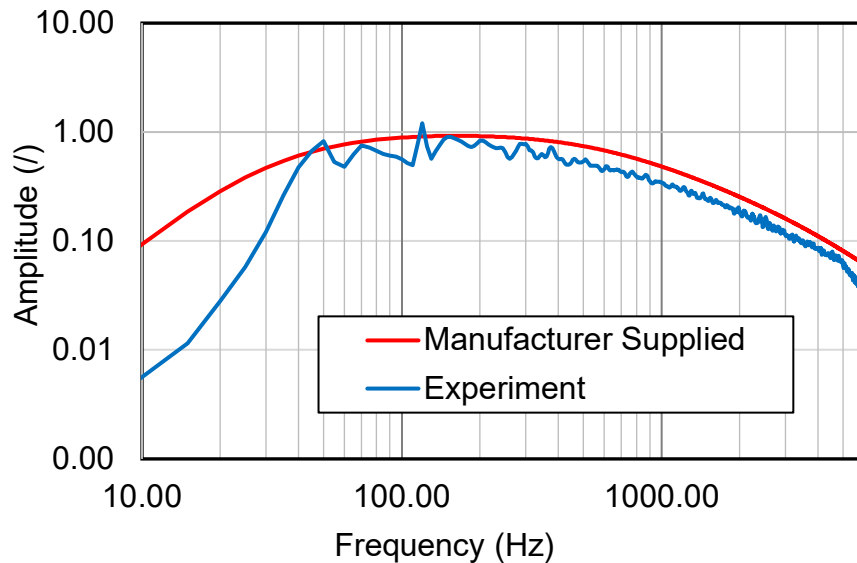
Figure 3.3 – Measured particle velocity sensitivity of the velocity sensor in the PU probe, 0-10000 Hz.
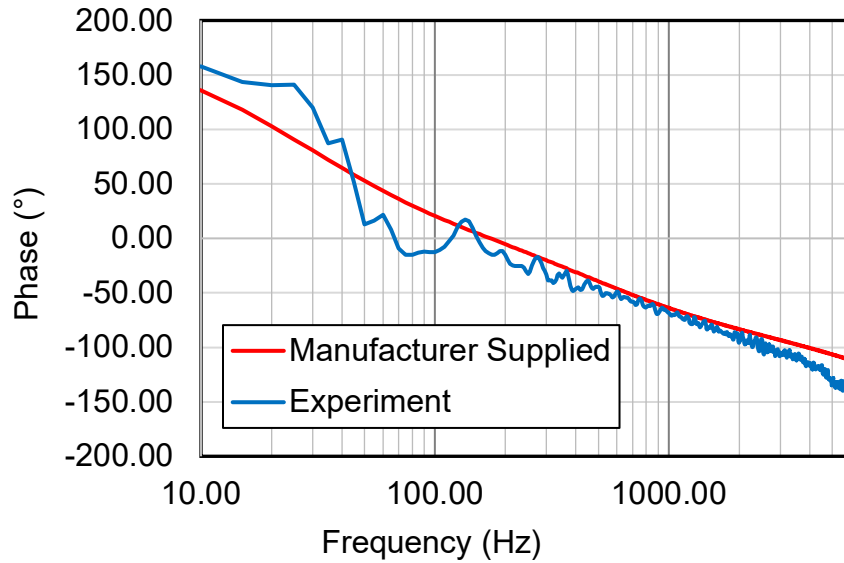
Figure 3.4 – Measured phase difference between of the velocity sensor in the PU probe and a quarter inch microphone, 0-10000 Hz.

3.2.3 Sound Intensity Comparison

The measurement of sound intensity was also checked for the PU probe by comparing to the two-microphone approach. Two microphones are spaced closely together and sound pressure is measured at both positions. Sound intensity is calculated from the two pressure measurements using Equation 2.9.
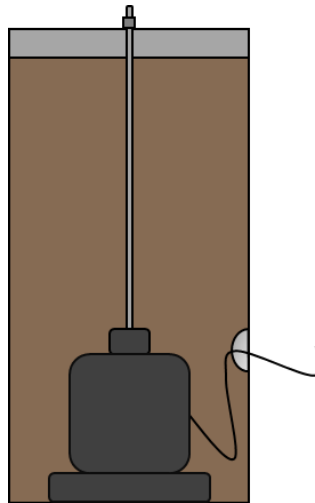
Figure 3.5 – Electromagnetic shaker used to excite aluminum plate for intensity measurements.

An aluminum plate was selected as the test article for the sound intensity comparison. A schematic of this test setup is shown in Figure 3.5. The plate and support structure are described in greater detail in Section 3.3.

Once mounted to the support structure, the shaker was used to vibrate the plate with white noise from 0-6000 Hz. The PU probe was then roved for thirty seconds across the surface of the plate at 15 cm away. Sound intensity was calculated using Equation 2.8 and time averaged over the surface. Likewise, the two-microphone probe was roved across the surface of the plate at 15 cm. Sound pressure was measured for each microphone and sound intensity calculated via Equation 2.19 was time averaged. Results are shown for each method in Figure 3.6.

The sound intensity measured with the PU probe and two-microphone method are correlate. Differences between curves at most frequencies are well under 2.5 dB above 250 Hz. These results demonstrate that the PU probe is properly calibrated. By measuring sound intensity on this simple baseline case, it can be seen that the PU probe corresponds well with standard practice. In the remainder of the chapter, the PU probe will be used to determine the radiation efficiency.
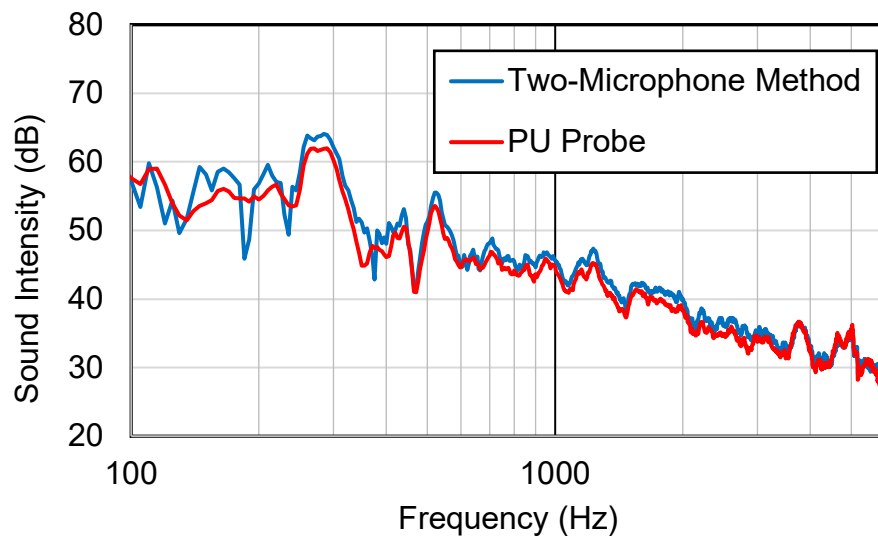
Figure 3.6 – Intensity scan results for PU probe and two-microphone method from 100-6000 Hz.

3.3 Aluminum Plate Case

3.3.1 Aluminum Plate Sound Power Test

A flat aluminum plate of thickness 3.175 cm was selected for the initial test case. By plugging appropriate material properties and thickness into Equation 2.5, the theoretical coincidence frequency of this plate is around 1300 Hz. The frequency range of interest is from 0 to 6000 Hz. A 50-lbs electromagnetic shaker was used to drive the panel and is more than sufficient since the panel is light. Figure 3.7 shows a photograph of the panel and overall dimensions.
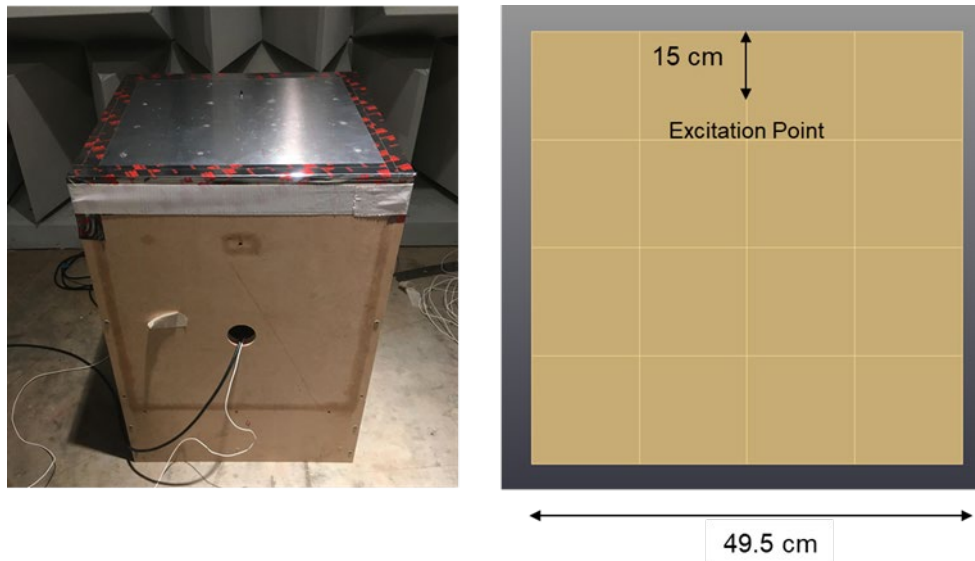
Figure 3.7 – Aluminum plate attached to wooden structure with shaker attached inside. Plate thickness of 3.175 mm.

The electromagnetic shaker was positioned inside the box shown in Figure 3.5. The box was made of 3/4-inch particle board. The plate was affixed to the top of the box using metallic tape. The shaker was attached to the panel at the position shown in Figure 3.7. It was located away from the center of the plate to avoid exciting the panel at node locations though the excitation position should not be as important at higher frequencies.

The radiated sound power from the plate was then measured with the PU probe at discrete locations. Discrete locations were chosen so that contour plots of the sound intensity could be prepared using the same data later. The sound intensity scan was

performed at a distance of 15 cm directly above the surface of the plate. Intensity was measured at the center of each patch point in the 4 x 4 grid shown in Figure 3.7 which yielded a total of 16 individual sound intensity values.

The time data was taken for thirty seconds at each location with five averages per second and the frequency resolution was set at 5 Hz. The white noise force excitation was controlled via Test.Lab and an amplifier.

After obtaining the sound intensity values as the discrete locations, sound power was calculated off the surface of the vibrating plate using Equation 2.10. Sound intensity was averaged over the surface of the plate and the multiplied over the area for the scan. Sound power was calculated and the measured sound power for the aluminum plate is shown in Figure 3.8.
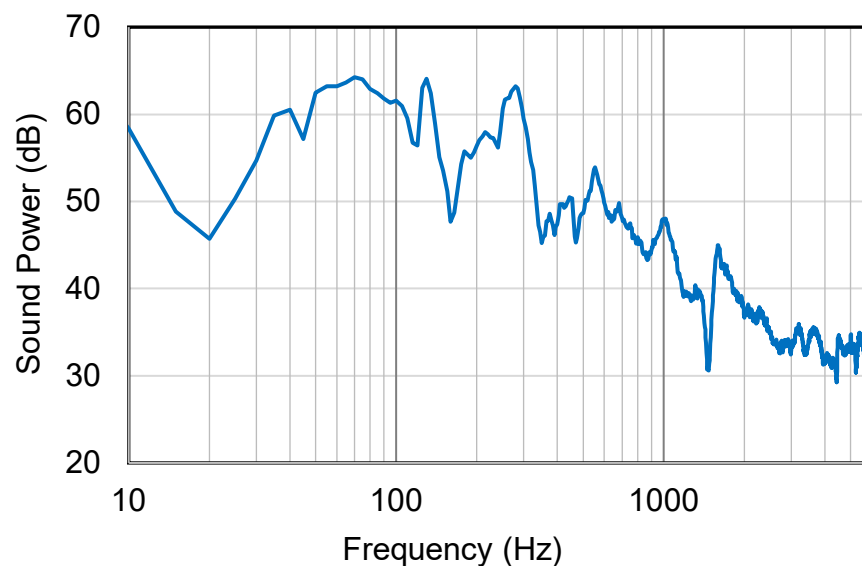
Figure 3.8 – Radiated sound power for the aluminum plate under white noise excitation. Frequency range of 10 - 6000Hz.

Sound power was determined at discrete locations above the surface of the plate. Siemens Test.Lab is capable of displaying the sound power as a contour plot as shown in Figure 3.9. This capability is very helpful for identifying the largest contributing sources. For

this example, it can be seen that the highest contributions are close to the excitation location.
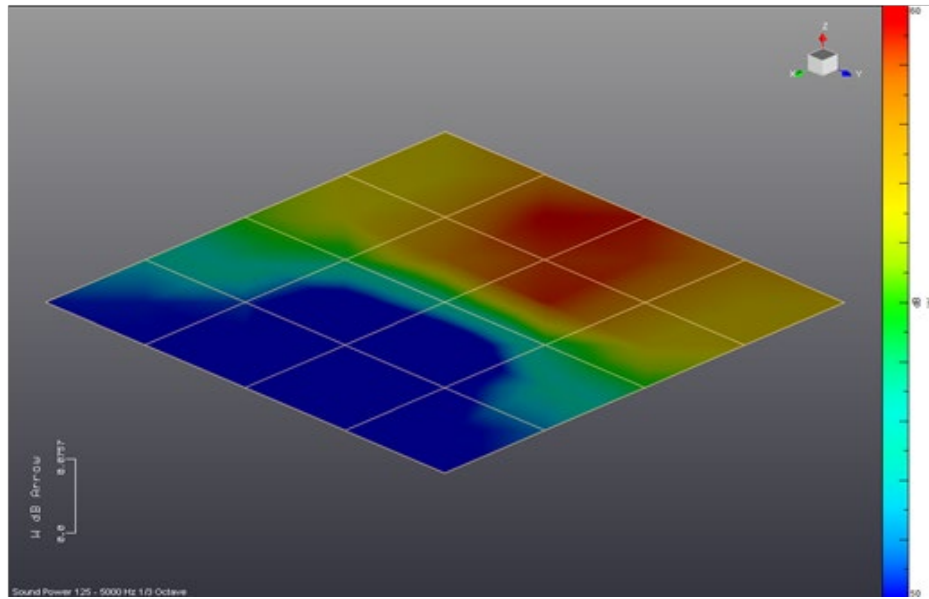
Figure 3.9 – Aluminum plate sound power map for summed third-octave bands 100 – 5000 Hz. Color scale is 10 dB red to blue.

3.3.2 Aluminum Plate Surface Velocity Test

To determine radiation efficiency, surface vibration was also measured on the aluminum plate. This was accomplished using the same test setup. Surface velocity was measured right after the sound power measurement to ensure that the operating conditions in no way changed between tests. This uniformity is extremely important – by slightly adjusting the input level on the amplifier or reapplying the metallic on the plate, surface velocity and sound power may be different changed between measurements. These errors should be minimal in this work because care was taken to ensure that neither the input forcing function or boundary conditions changed between tests.

Moreover, surface velocity was measured with two separate methods; an accelerometer array and by roving the PU probe near the surface of the plate. For the standard method, an accelerometer array was directly attached to the surface of the structure at the center of each patch as shown in Figure 3.7. Acceleration was measured via the accelerometer

array for thirty seconds at each center location. The average velocity was then obtained for the 16 measurements. Dummy masses were utilized to prevent mass loading effects since only 6 accelerometers were available for the measurement.

For the PU probe measurements of surface velocity, the PU probe was placed 0.5 cm away from the center of each patch. Since particle velocity rapidly decays as a function of distance away from a source, distance was minimized to reduce error between the particle velocity sensor in the PU probe and corresponding accelerometer measurements. To reduce human error, the PU probe was positioned using a microphone stand at the specified distance above the vibrating plate. The PU probe was moved to each discrete location and data was obtained and averaged for 30 seconds. Average particle velocity at 0.5 cm above the plate was then calculated by spatially averaging the data at all 16 locations.

Comparisons between the average surface velocity measured with the accelerometer array and the PU probe are shown in Figure 3.10. This difference remains fairly constant with frequency and is approximately 3 dB. This can likely be attributed to the distance between particle and surface velocity. Note that the results converge at very high frequencies.
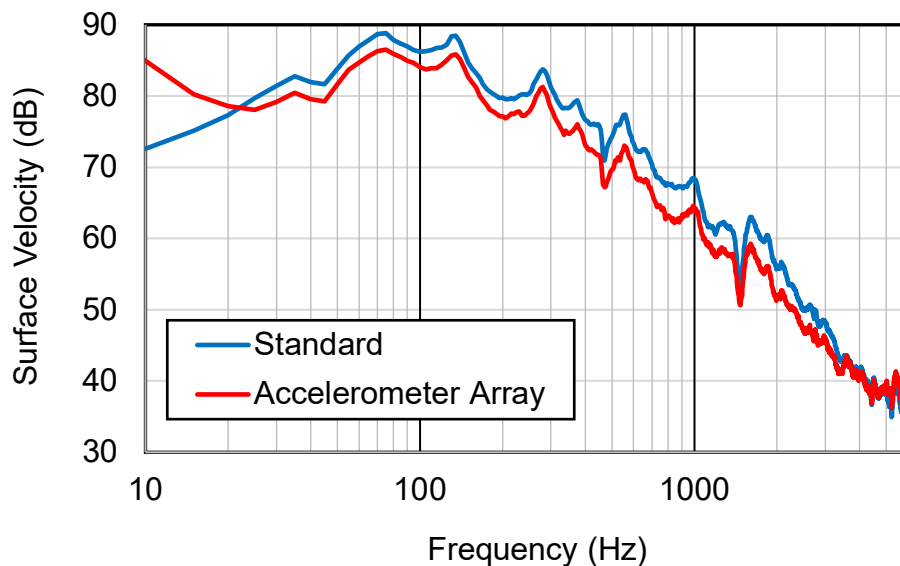
Figure 3.10 – Surface velocity comparison between PU probe and accelerometer array on aluminum plate. 10-6000 Hz

29

3.3.3 Aluminum Plate Radiation Efficiency

After completing both the surface velocity determination and sound power mapping for the aluminum plate, radiation efficiency was calculated utilizing Equation 2.1 for both the standard method and PU probe measurements. Figure 3.11 shows these results. Since the PU probe measured a lower surface velocity, the calculated radiation efficiency is a few dB higher than the standard measurement. Hence, the denominator in Equation 2.1 is lower if the PU probe is used which correspondingly increases the radiation efficiency by a similar amount.
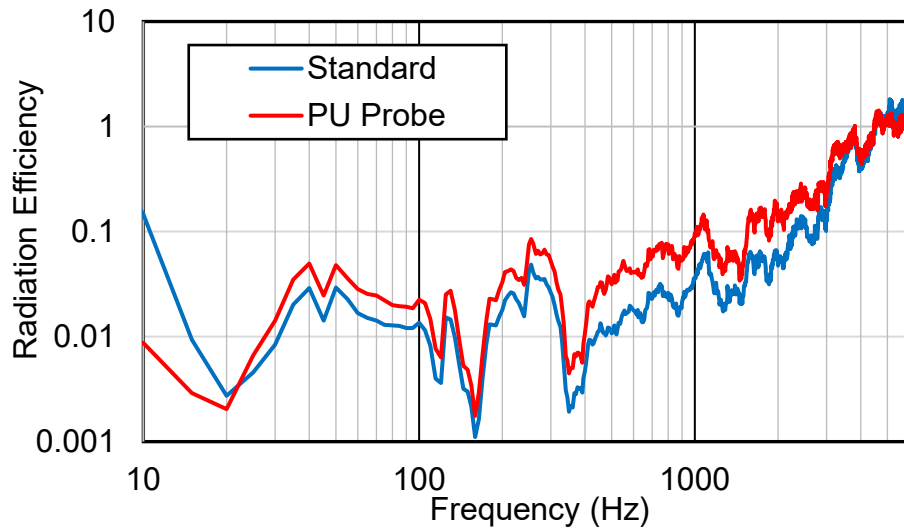
Figure 3.11 – Comparison of radiation efficiency for aluminum plate.

Note that the radiation efficiency increases to close to unity at around 3000 Hz which is much higher than the coincidence frequency which is predicted to be 1300 Hz using Equation 2.5. However, Equation 2.5 does not take into account the boundary conditions of the plate. In summary, the radiation efficiency error hovers around 3 dB except at the very high frequencies. As an engineering method, it is an acceptable alternative to ISO-7849 for this case.

3.4 Stainless-Steel Plate Case

3.4.1 Stainless-Steel Sound Power Test

The second test case is much thinner 1 mm thick stainless-steel plate mounted to the same wooden support structure as before. For this test case, a 3 X 3 set of 9 points was used for sound power mapping. The test setup is shown in Figure 3.12 and is identical to the Section 3.3 measurement but with the thinner stainless-steel plate. Per Equation 2.5, the coincidence frequency is approximately 3700 Hz. From the coincidence frequency calculation, the stainless-steel plate is anticipated to have a lower radiation efficiency than the aluminum plate.
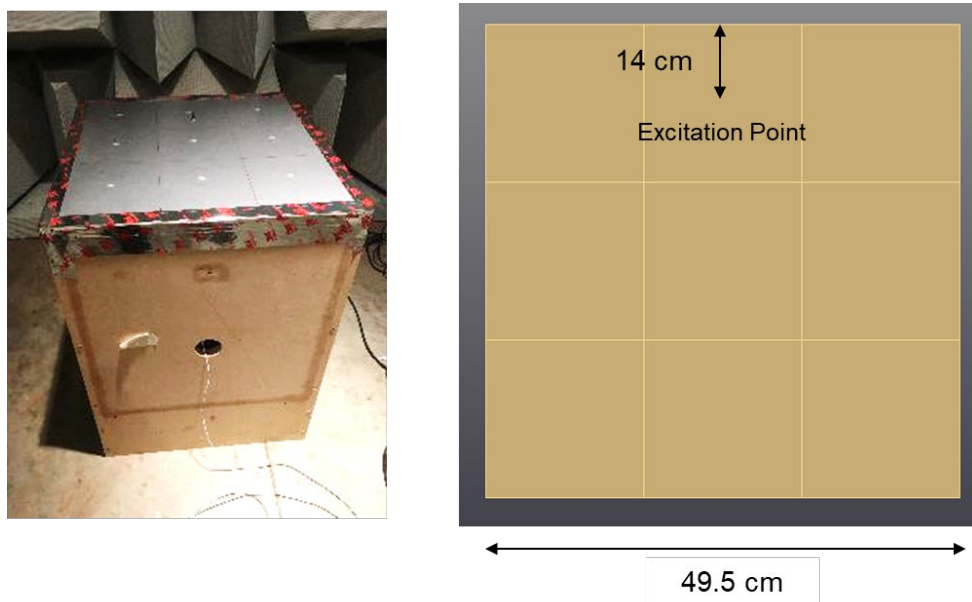
Figure 3.12 – Stainless steel plate test setup. Stainless plate thickness 1mm.

Sound intensity was measured with the PU probe in the same manner described in Section 3.2.1. The plate was excited by the electromagnetic shaker using white noise from 0 to 6000 Hz. The probe positioned at the center of each patch and sound intensity was measured. Data was time averaged for 30 seconds at each location. The spatially averaged sound intensity was then determined over the surface of the plate. The radiated sound power was then calculated by multiplying the average sound intensity by the area

of the scanning surface in a manner analogous to ISO-9614-2. The sound power is plotted versus frequency in Figure 3.13.
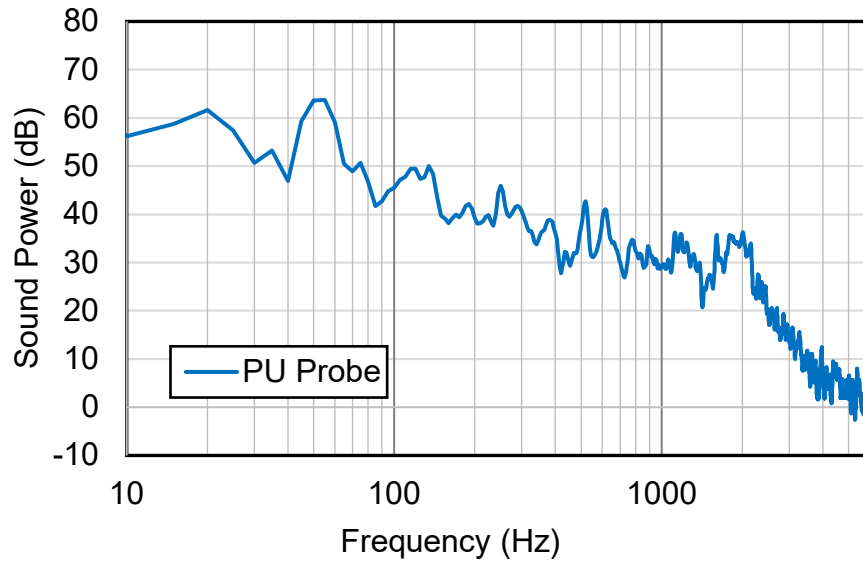
Figure 3.13 – Sound power measurements for stainless steel plate, 10-6000 Hz.
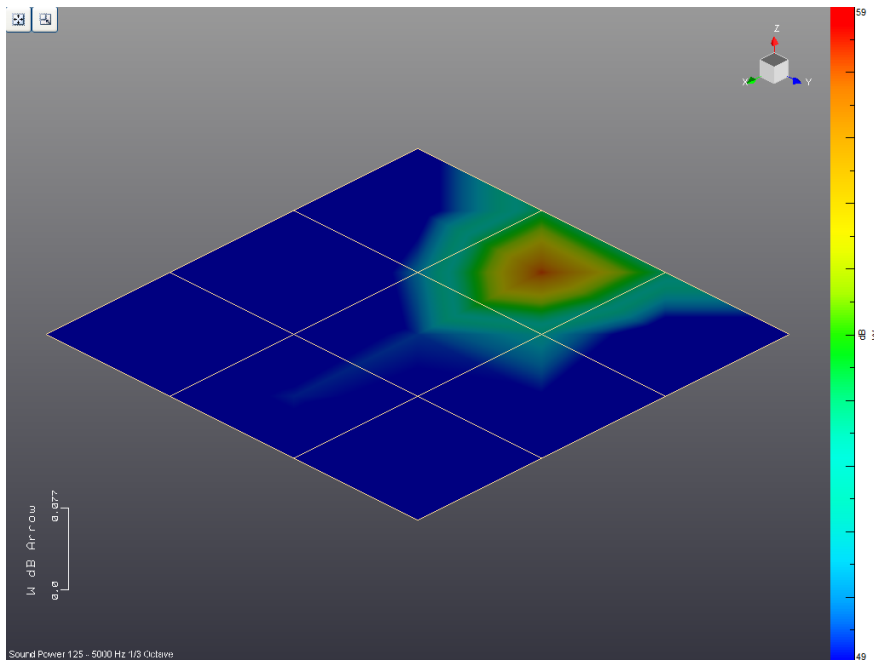
Figure 3.14 – Total sound power measurements for stainless steel plate from 100-5000 Hz, summed 1/3 octave bands. Same 10 dB scale as in Figure 3.9.

Figure 3.14 shows the sound power mapping for the stainless-steel plate. One-third octave band results are summed in this plot. Note that location around the stinger contributes most to the overall sound power. However, the contribution likely varies as a function of frequency so no sweeping conclusions should be made.

3.4.2 Stainless-Steel Surface Velocity Test

After completing the sound intensity mapping for the thinner stainless-steel plate, the surface vibration methods applied to the aluminum plate were repeated on the new plate. Accelerometer measurements were made at the center of each patch and the PU probe was used to measure particle velocity at a distance of 0.5 cm away. A single accelerometer was roved from position to position. This procedure was likewise followed for the PU probe. Accelerometer and PU probe measurements were spatially averaged.
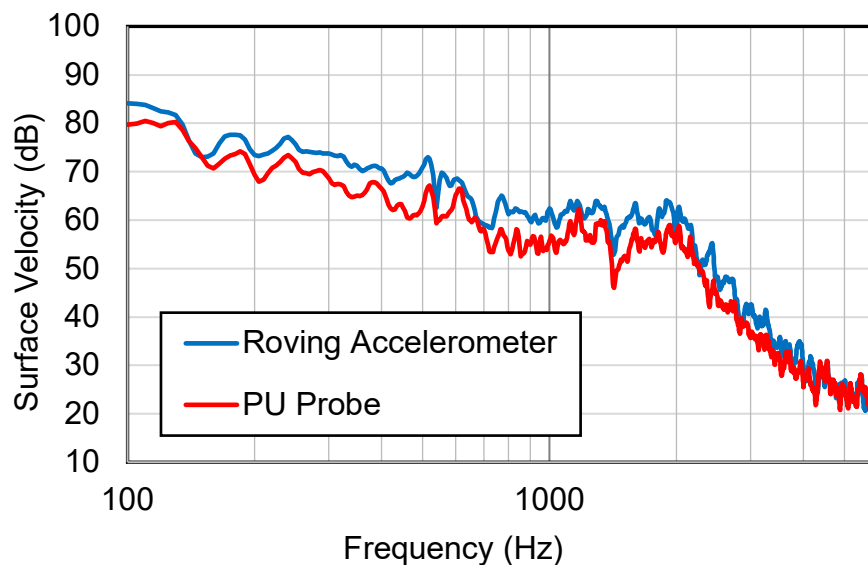
Figure 3.15 – Average surface velocity results for stainless steel plate configuration. 10-6000 Hz.

Figure 3.15 compares the spatially averaged surface velocity measured with an accelerometer to the spatially averaged particle velocity measured with the PU probe. Agreement is similar to the aluminum plate case, and it can be seen that the PU probe measures a few dB low at most frequencies. By switching from 16 discrete measurement

locations to 9, accuracy does not seem affected. Also, the effect of mass loading seemed to be negligible since the accelerometers were removed for PU probe measurements.

3.4.3 Stainless-Steel Radiation Efficiency

The radiation efficiency was determined using both the standard and PU-probe approaches. Results are compared in Figure 3.16. It can be observed in Figure 3.16 that radiation efficiency is much lower for the stainless-steel plate as is anticipated. Similar to the aluminum plate, the lower measured surface velocity using the PU probe results in a 2-4 dB higher radiation efficiency calculation. Notice that the radiation efficiency does not approach unity up to 5000 Hz..
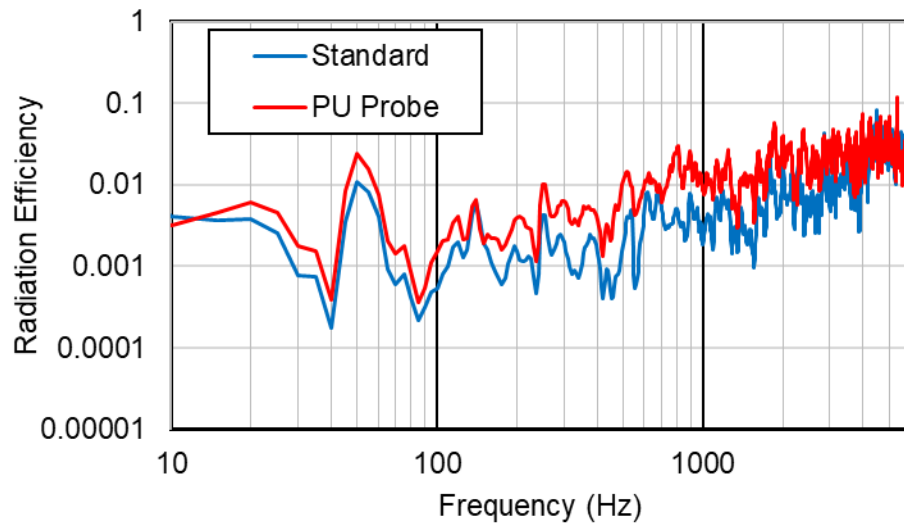
Figure 3.16 – Radiation efficiency results for both standard and PU probe on the stainless-steel plate, 10-6000 Hz.

3.5 Oil Pan Case

3.5.1 Oil Pan Sound Power Test

As seen in the previous sections, the PU probe can function as an alternative method for radiation efficiency determination. In Sections 3.3 and 3.4, simple geometries in the form of thin metallic plates were explored. While these plates are typical of plates on enclosures and HVAC ductwork, most mechanical structures are not so simple. To meet performance and mechanical expectations, mechanical components frequently have very complicated geometries. With this in mind, a few industrial applications have been selected to further evaluate the accuracy of the PU-probe for measurement of radiation efficiency.

The first of these applications is a ribbed, aluminum oil pan. By functioning as a reservoir for engine oil, this cover is bolted to an engine block in application. As the engine operates, internal combustion and mechanical forces propagate through the engine block to the oil pan which in turn radiates noise. By understanding the radiation efficiency of the oil pan, the manufacturer can reduce the propagation path between force excitation and airborne sound power.
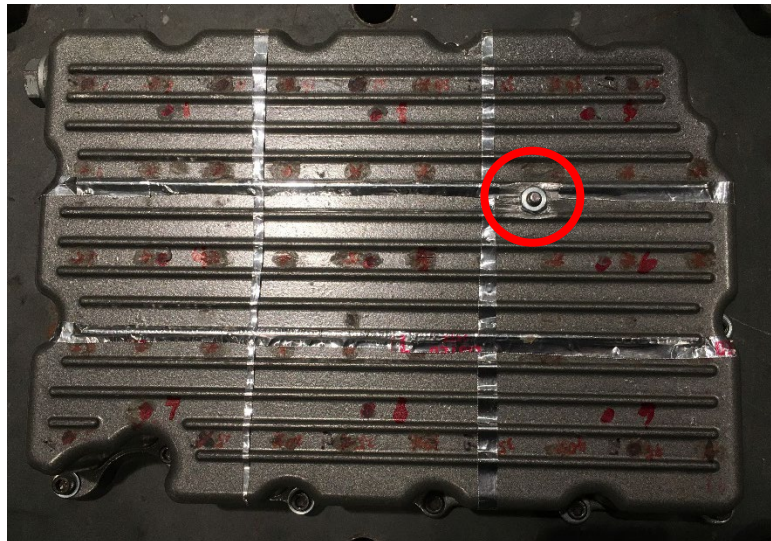
Figure 3.17 – Aluminum oil pan mounted to massive mounting block to simulate engine block boundary conditions. Stinger location is circled in red.

The ribbed oil pan was mounted to a 32 kg (70 lbs) steel plate. The electromagnetic shaker utilized in previous sections was selected as the force excitation. The oil pan was divided into a 3 X 3 grid and measurements were made at the center of each of the 9 patches. The shaker was attached between patches 3 and 6 as shown in Figure 3.17. Figure 3.17 shows the oil pan attached to the 32 kg steel plate. Note that the oil plan is bolted to the plate at each of the prescribed mounting holes.

Figure 3.18 – Imaginary box constructed around the oil pan for sound intensity scan. Imaginary surfaces are 30 cm from each face of the pan.

In order to determine the oil pan's radiation efficiency, a sound intensity scan was first performed to find radiated sound power. To perform the scan, a cuboid grid was constructed with surfaces that were 30 cm away from each face of the cover as shown in Figure 3.18. White noise excitation was used and the PU probe was roved across the surface of each imaginary plane to determine the sound power. The average sound intensity was measured through each plane and the sound power was determined by multiplying the intensity by the area. Data was time averaged for 30 seconds during each sweep. The sound power is plotted versus frequency in Figure 3.19.
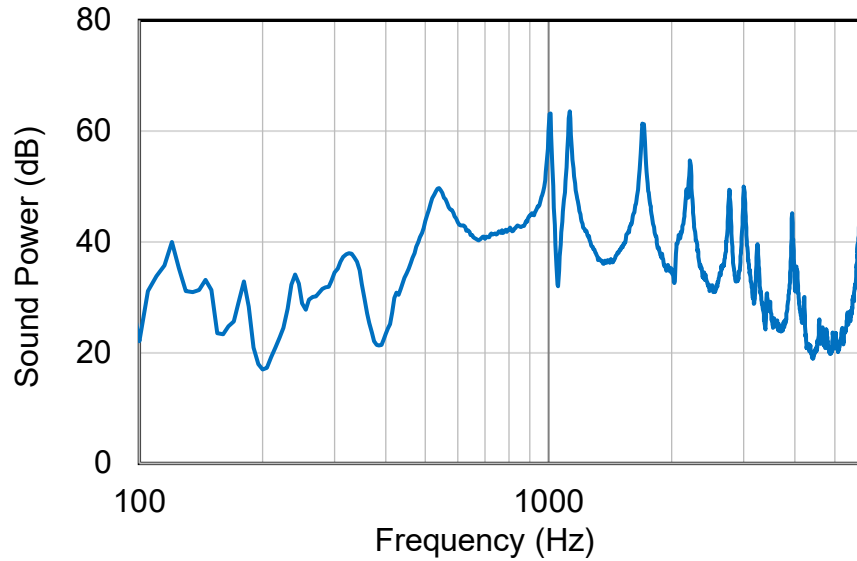
Figure 3.19 – Oil pan sound power results from 100-6000 Hz.

3.5.2 Oil Pan Surface Velocity Test

The surface vibration was the measured by roving a single accelerometer along the plate. Measurements were made at the center of each patch. The oil pan is stiff and massive so the effect of mass loading was expected to be negligible. Data was collected and averaged for 30 seconds at teach position. The nine measurement points should be sufficient according to ISO-7849. The surface area of the oil pan is under 1 m^2 and for this surface area, five measurement points are recommended per ISO-7849 [2].

Particle velocity was measured with the PU probe at a distance of 0.5 cm from the surface. The PU probe was mounted on a microphone stand to ensure that the distance between prove and surface was kept constant at 0.5 cm. White noise excitation up to 6000 Hz was input. Data was collected and averaged for 30 seconds at the center of each patch. The particle velocity was then spatially averaged.

The surface and particle velocity at a distance of 0.5 cm are compared in Figure 3.20. The PU probe measurements are about 3 dB lower than the surface vibration. This is likely a result of particle velocity decaying as the distance from the plate increases. Also, it is notable that the resonant peaks dropped in frequency by about 5 Hz. This is almost

37

certainly a result of mass loading. However, this slight reduction in frequency will only slightly impact the radiation efficiency predictions.
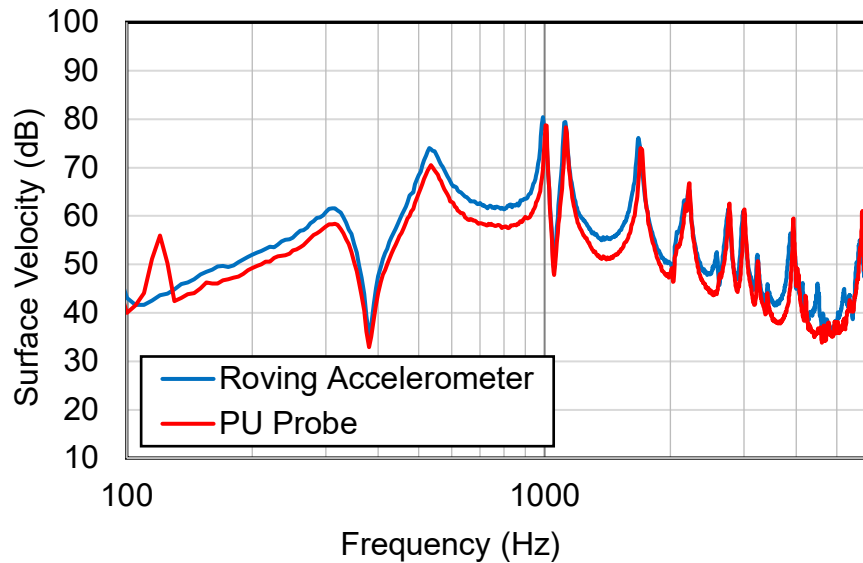
Figure 3.20 – Comparison of surface velocity results for aluminum oil pan from 100-6000 Hz.

3.5.3 Oil Pan Radiation Efficiency

Using the sound power and surface vibration data, radiation efficiency was calculated according to Equation 2.1. Radiation efficiency results are plotted in Figure 3.21 for the frequency range of interest. Results between the standard approach and the PU probe correlate well though there is approximately a 3 dB difference consistent with the prior two plate examples. The lower PU probe results are again a result of the lower average surface vibration measurement using the PU probe.

There are some advantages in using the PU probe in this example. As noted earlier, mass loading does slightly shift some of the frequency peaks lower in frequency. Additionally, there is some difficulty in mounting accelerometers to the cover because of the ribbing, so a non-contact approach is easier to use. Finally, the test case suggests that the radiation

efficiency measurement can be improved if the particle velocity measurement is adjusted. This topic will be explored further in Chapter 4.
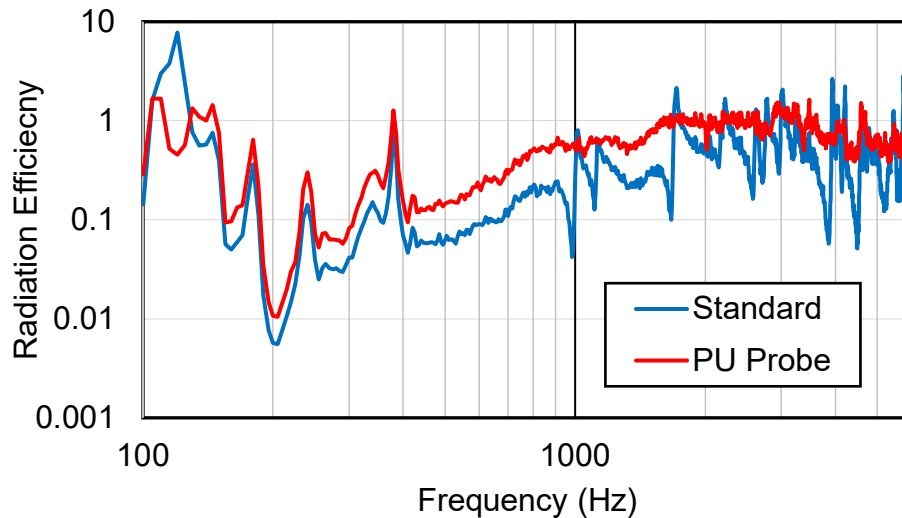
Figure 3.21 – Oil pan radiation efficiency results from 100-6000 Hz for the PU probe and standard methods.

3.6 Gas Tank Case

3.6.1 Gas Tank Sound Power Test

The final test case considered is a field test where the radiation efficiency of the gas tank on an internal combustion engine is measured. This was accomplished by considering the gas tank on an internal combustion engine. The previous plate test cases consisted of one forcing function (the shaker) and one acoustic source (the plate). The internal combustion engine (420 cc) has several noise generating components. Some of these components are in close proximity with each other. The gas tank is a good candidate component because it receives vibratory energy through other components but is not exposed to larger dynamic forces like piston slap and combustion.

Measuring the radiation efficiency is difficult for a component because it is difficult to accurately measure sound power using a sound intensity probe in the presence of other sources. Nearby sources add noise to the measurement. However, the PU probe is very

directional and sound power can be accurately determined even if other sources are dominant.

Figure 3.22 shows a photograph of the gas tank and the measurement grid. Notice that the geometry of the gas tank is cuboidal. Four sides of the gas tank are exposed. The bottom is nestled against the engine block and the left side next to the muffler and intake. The four exposed surfaces were discretized into a 3 X 3 grid and measurement locations were positioned at the center of each grid square. An imaginary box, 15 cm (6 in) away from each exposed surface, was constructed for measuring sound intensity. If the box is larger, other sources such as the fan and intake manifold will be included in the sound power measurement. While near field effects are not guaranteed to be avoided, the selected distance of 15 cm is selected a compromise. This is a common issue faced when measuring sound intensity in a field with several closely spaced sources.
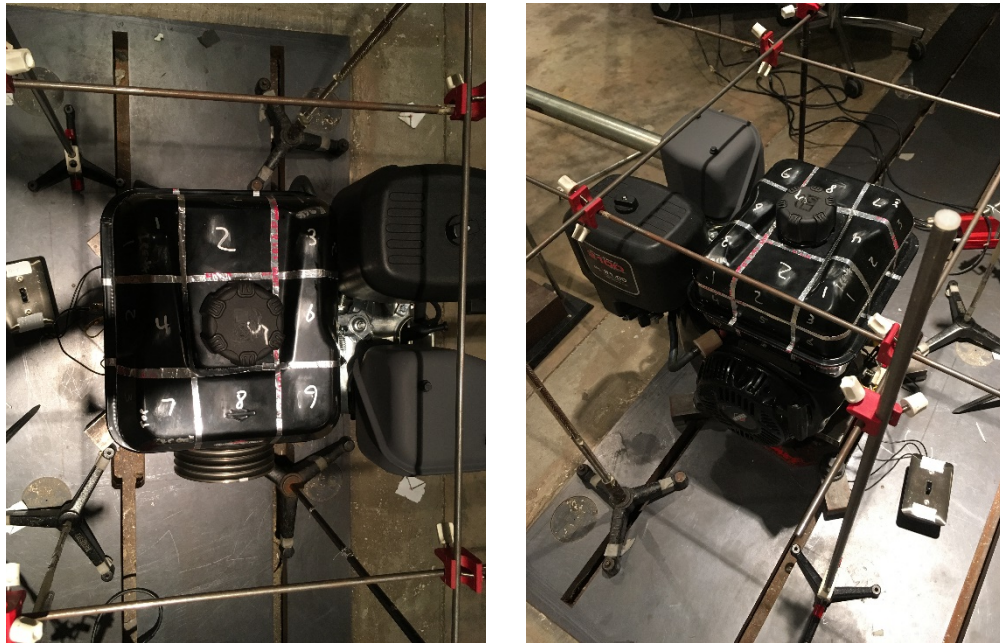
Figure 3.22 – 420cc engine gas tank. Notice that only 4 sides of the tank are exposed and have measurable contributions.

Typical operating speeds for this engine are in the range of 2000 to 4000 RPM, a safe steady-state operating speed of 2700 RPM was selected as the operating condition. The

engine was mounted to a stand which was in turn rigidly fixed to a bed plate for safety reasons. The engine speed was monitored with an optical tachometer and was recorded using a tach channel on the SCADAS. An inertia disk was attached to the crankshaft in order to load the engine by a small amount. By adding this loading, the inertia disk simulates being attached to a driveshaft and stabilizes the engine with boundary conditions similar to actual operation.

Sound intensity was obtained on the running engine using two separate methods. It was first measured at 15 cm away from each exposed surface of the tank. Sound pressure and particle velocity were measured normal to each imaginary surface at 15 cm away for thirty seconds with the PU probe in a sweeping manner. The frequency range of interest was 125 to 5000 Hz and data was taken in third-octave bands. Third-octave bands are desirable over narrowband in cases where time harmonic frequencies are dominant. For the combustion engine, strong harmonics occur at frequencies corresponding to engine speed. By summing the data in one-third octave bands, the calculated sound power and radiation efficiency is easier to understand visually on a graph. Sound intensity was calculated for each surface with Equation 2.8. After intensity was averaged across the surface of the imaginary box, sound power was obtained via Equation 2.10 by multiplying average sound intensity by surface area.

Sound intensity was also measured closer to the vibrating surfaces of the gas tank. Even though near-field effects affect the measurement close to the source, a scaled-down scanning box at 1.5 cm from each surface of the tank was constructed. By encompassing a smaller area during the intensity scan, other components generating unwanted contributions can be eliminated. After the new scanning surface was created closer to the gas tank, the PU probe was roved for thirty seconds across each surface. Sound pressure and particle velocity were determined for each surface and sound power was measured as before.

Results for both the near-field and far-field power are plotted in Figure 3.23. Comparing the sound power between both scans, large discrepancies are present. The sound power measured in the far-field is much larger than that measured in the near field especially at

frequencies below 630 Hz. By increasing the area of the scanning surfaces, the sound power measured at a distance of 15 cm is likely contaminated by sources other than the gas tank. With this in mind, sound power obtained close to the surface of the tank is used for determining radiation efficiency.
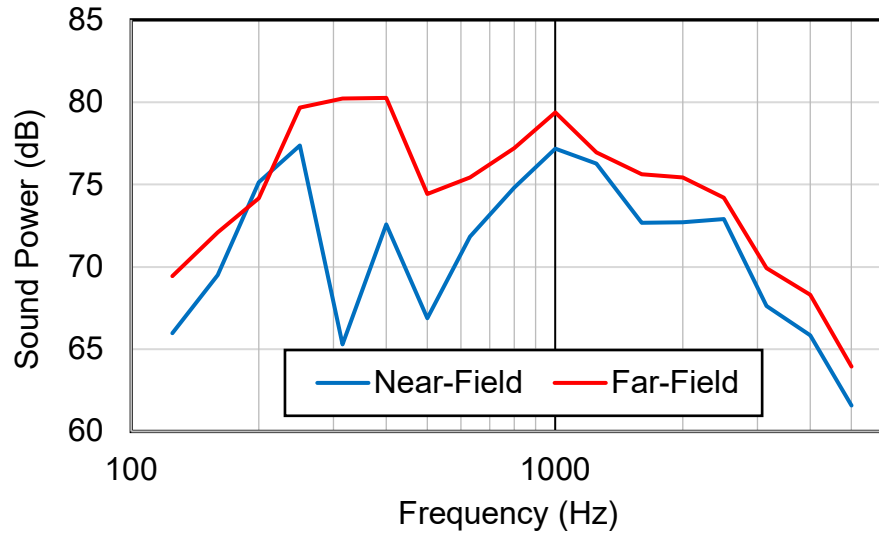
Figure 3.23 – 420cc engine gas tank sound power results in third-octave bands, 125-5000 Hz.

3.6.2 Gas Tank Surface Velocity Test

The surface acceleration was measured using 9 accelerometers. All sensors were attached to the surface of the tank during all measurements to insure consistency of mass loading. After one side was completed, the entire array of accelerometers was moved to a different face on the gas tank. Average acceleration was determined for each face and surface velocity was obtained using Equation 2.7.

The PU probe was then used to measure particle velocity at the center of each patch 1.5 cm away from the surface of the gas tank. Instead, the PU probe was attached to an aluminum rod and held in hand. This complex geometry required more finesse in keeping the probe normal to the tank's surface and use of a microphone stand was unfeasible. As such, controlling the distance away from the surface of the vibrating tank was difficult when compared to the plate and oil pans tests.

42

After the particle velocity at 1.5 cm away was obtained at all thirty-six measurement points, average particle velocity was calculated for the entire exposed surface. Figure 3.24 shows the third-octave band frequency plots for surface velocities obtained with the accelerometer array and the PU probe.
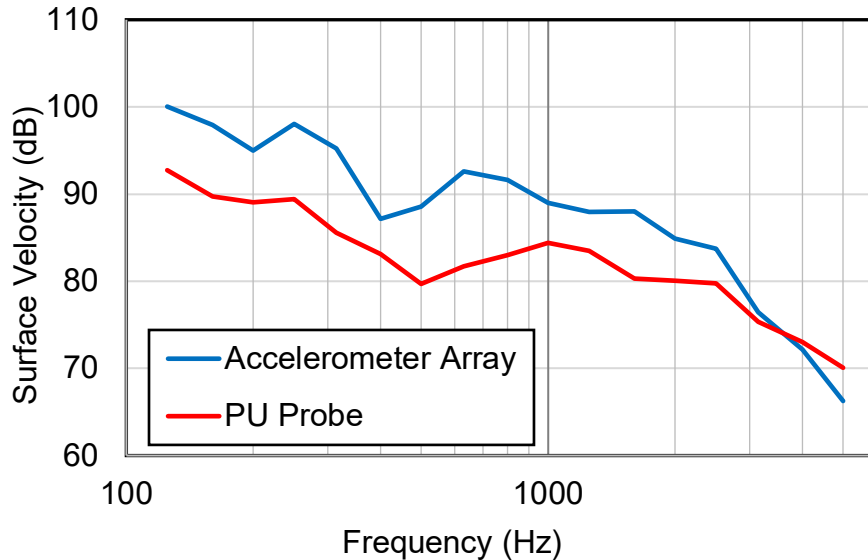
Figure 3.24 – Gas tank surface velocity results for the 420cc engine. 125-5000 Hz.

3.6.3 Gas Tank Radiation Efficiency

Using the surface velocity and sound power measurements at 1.5 cm away from each surface of the tank, radiation efficiency was calculated according to Equation 2.1. Figure 3.25 compares the radiation efficiency measured using each approach. The error between the methods is on the order of 10 dB at some frequencies. As anticipated, the radiation efficiency measured using the PU probe is high due to the inaccurate measurement of surface vibration. Errors are higher in this case because the PU probe is located further away from the vibrating surface. However, it was hypothesized that the PU probe results could be corrected so that correlation was improved.
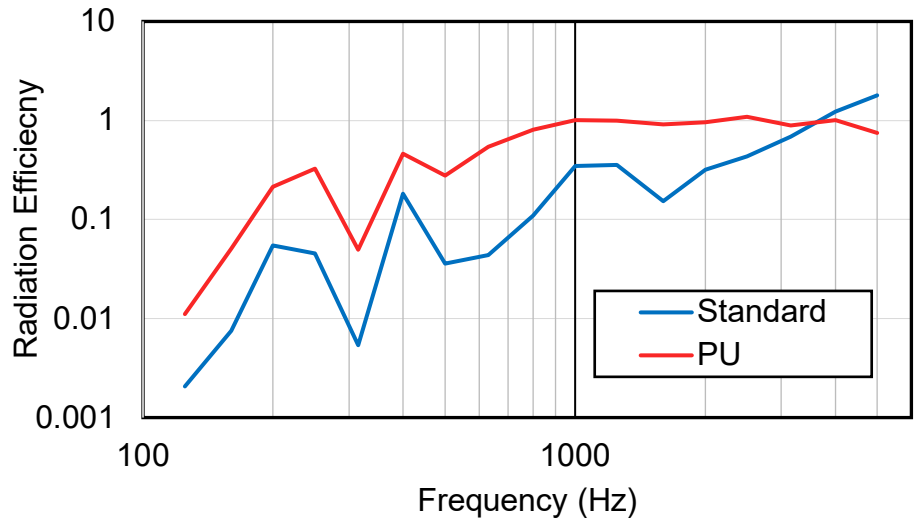
Figure 3.25 – Third-octave band frequency plot for gas tank radiation efficiency results from 125- 5000 Hz.

CHAPTER 4 RESULTS AND DISCUSSION

4.1 Discussion on Surface Velocity

The results in the prior chapter indicated that particle velocity decays rapidly with distance from the vibrating surface. This effect was investigated using Patch 6 on the aluminum plate. The particle velocity was measured at different distances from the source and compared to surface velocity. The ratio of the measured particle to surface velocity is shown in Figure 4.1. It can be seen that the ratio decreases significantly with distance away from the source.
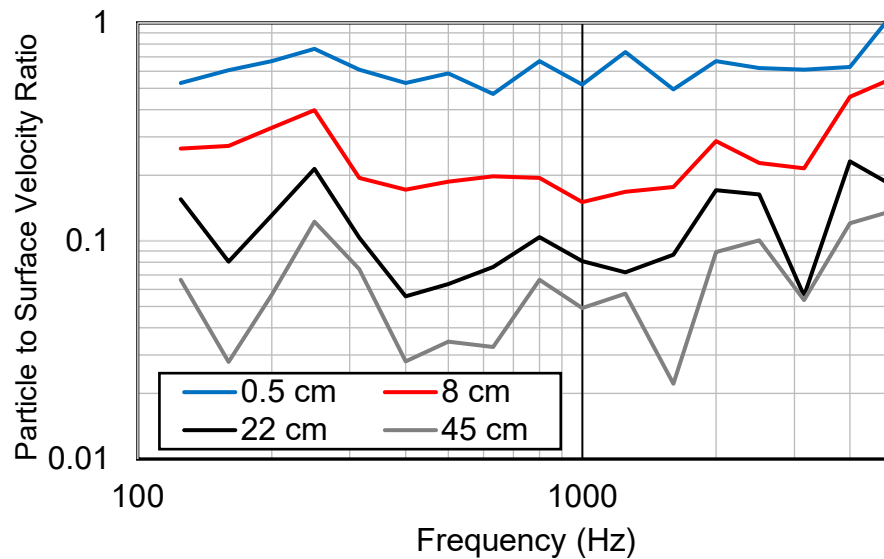
Figure 4.1 – Aluminum plate Patch 6, ratio of surface velocity and particle velocity measured at various distances away. 0-5000 Hz, third-octave bands.

Based on these results, a correction method is proposed to adjust the particle velocity measured with the PU prove to better match the actual surface velocity. Though an analytical relationship could be developed, the relationship between particle and surface velocity likely depends on the surface velocity. Instead, a simple measurement correction is recommended. The surface velocity $v_n(x = 0)$ at a position on the vibrating surface is measured with an accelerometer and compared withthe particle velocity $u_n(x)$ at some distance away from the surface. A transfer function is measured between the two and the

amplitude is taken. With n equal to the patch number, the transfer function H is expressed
as

$$H = \frac{v_n(x = 0)}{u_n(x)} \qquad (4.1)$$

This transfer function serves as a distance and frequency-based correction and can be measured for various distances away from the source. By measuring the average surface velocity across the entire surface of the source at a constant distance x, the average surface velocity can be determined by multiplying the average particle velocity across the surface by the transfer function shown in Equation 4.1. This transfer function amplitude serves as a simple correction for the measured particle velocity. This measurement is easily completed and can be considered a calibration for the PU probe.

The main concern that can arise from utilizing one point on a vibrating surface to correct the PU probe is where to place the accelerometer. Regardless of the selected position, it is inevitable that the position will lie on the node line of certain modes. This lack of measured vibration will lead to inaccurate data at certain frequencies. There are two ways to mitigate this issue. One method is to measure the surface vibration at several positions and average, but that increases the measurement time and complexity. Alternatively, a running average of the transfer function can be performed to smooth the result. This method is more advantageous since transfer functions for radiation problems are anticipated to be smooth. By using a running average, peaks and troughs resulting from plate resonances will be smoothed.

4.2 Surface Velocity Corrections

4.2.1 Aluminum Plate Velocity Corrections

The particle to surface velocity ratio is shown in Figure 4.2 for the aluminum plate. Particle velocity is measured 0.5 cm from the plate surface. If a 200 Hz running average is applied, the smoothed curve also shown in Figure 4.2 is obtained. Note that the peaks and troughs in the narrowband transfer function are smoothed out which yields a smooth correction curve. It is recommended that the location selected for correction not be too close to the excitation location or a fixed edge.

Figure 4.2 – Transfer function between particle velocity at 0.5 cm away and surface velocity at Patch 6 for aluminum test case. 100-6000 Hz.

With this velocity correction curve, the average particle velocity was corrected. This correction can be expressed as

$$v_{avg} = u_{avg} \times H \quad (4.2)$$

47

where u_{avg} is the average measured particle at $x = 0.5$ cm and H is the correction transfer function. After applying the correction, the surface velocity measured with the PU probe correlates very well with the surface vibration measured using accelerometers as shown in Figure 4.3. Differences are less than 2 dB at most all frequencies.
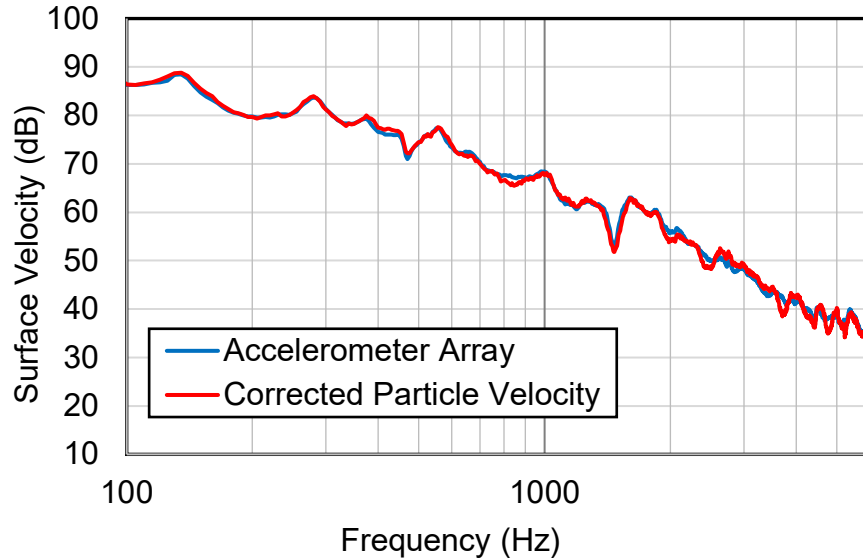
Figure 4.3 – Corrected velocity measurements for the aluminum plate test case from 100-6000 Hz. Notice that the FRF-Correction Method for the PU probe yields higher accuracy than the uncorrected particle velocity.

Note that the proposed approach is straightforward and requires minimal additional data. If the distance from the plate is chosen optimally, it is possible that one measurement surface will be sufficient. Based on this initial success, the method was used to determine the surface vibration for the other 3 examples.

4.2.2 Stainless-Steel Plate Velocity Corrections

A similar velocity correction was also applied to the 1 mm stainless-steel plate. The ratio of the surface to particle velocity is plotted versus frequency in Figure 4.4. A 200 Hz running average was again applied to smooth out any discontinuities. The correction curve and even the smoothed curve are not as flat as the result for the 5 mm aluminum plate. These discontinuities likely arise as a result of the accelerometer being located at

node lines of the mode shapes of the plate. The chance of this occurring increases at higher frequencies as the structural wavelength decreases.
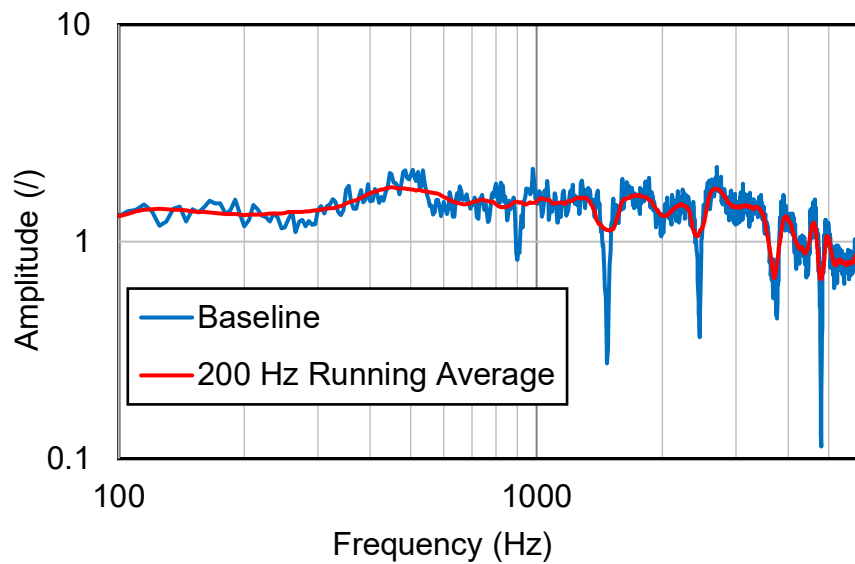

Figure 4.4 – Transfer function between particle velocity at 0.5 cm away and surface velocity at Patch 6 for stainless-steel test case. 100-6000 Hz.

Figure 4.5 – Corrected velocity measurements for the stainless-steel plate test case from 100-6000 Hz.

The corrected particle velocity results are compared to the accelerometer measurements in Figure 4.5. The agreement is acceptable even at higher frequencies. The discrepancies at 1700 and 2700 Hz result from measuring at node lines on the plate since the surface vibration is very low at these positions. This results in an over correction, but taking a running average reduces the amount over correction. One advantage of a particle velocity measurement is that there are no gaps in vibration data at the node lines.

4.2.3 Oil Pan Velocity Corrections

The particle velocity was likewise corrected for the oil pan test case. Patch 8 was selected since it was not near the excitation position or the edges. The ratio of the surface vibration to particle velocity is compared in Figure 4.6 as a function of frequency. A 200 Hz running average is again used and a relatively flat calibration curve is identified. There are some peaks at higher frequencies. These occur at frequencies where the surface vibration is low.
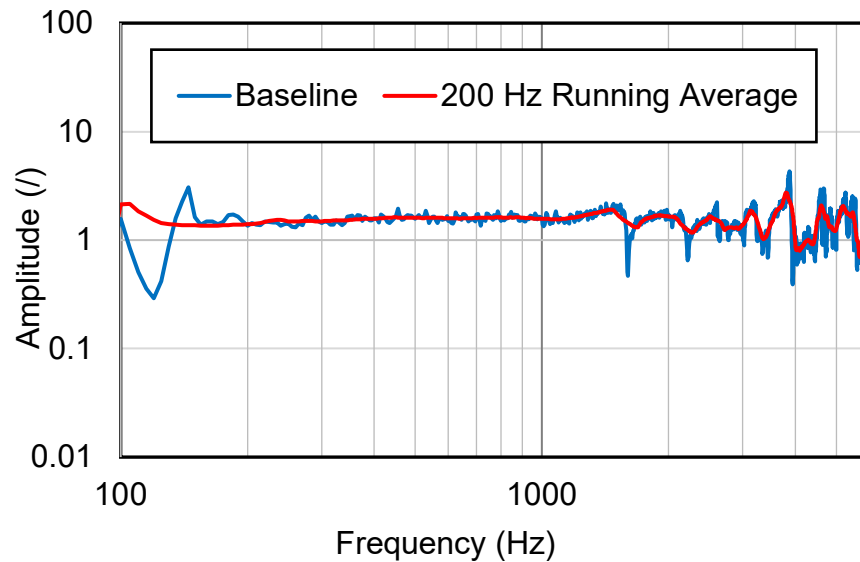
Figure 4.6 – Transfer function between particle velocity at 0.5 cm away and surface velocity at Patch 8 for oil pan test case. 100-6000 Hz.

The error between the corrected and measured particle velocity is shown in Figure 4.7. Agreement is excellent at most frequencies.
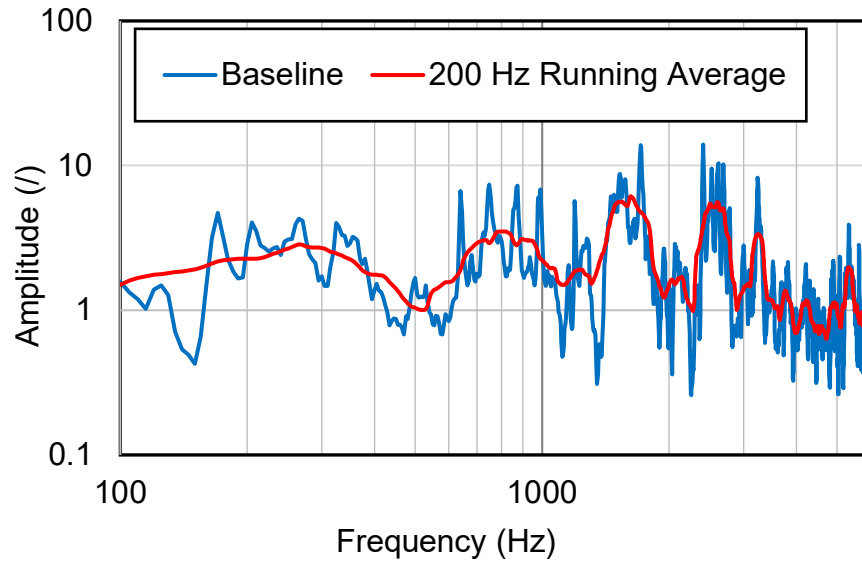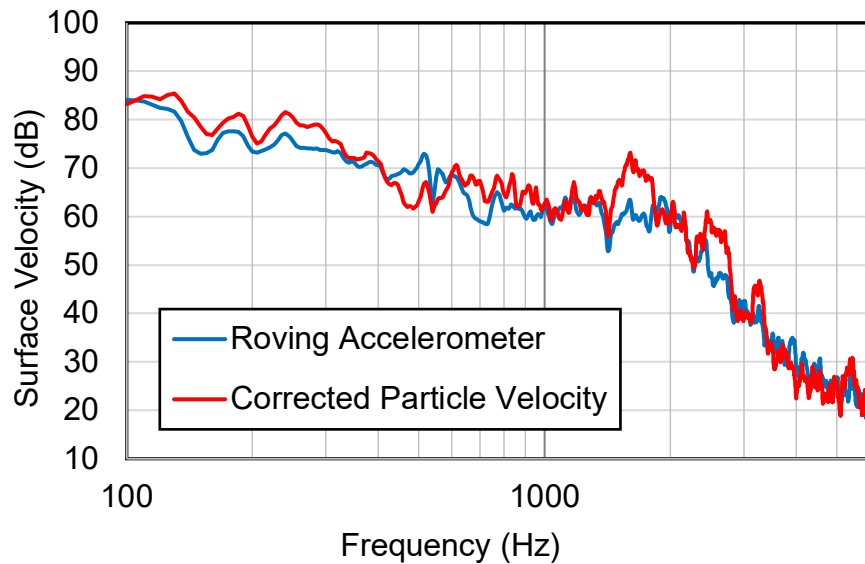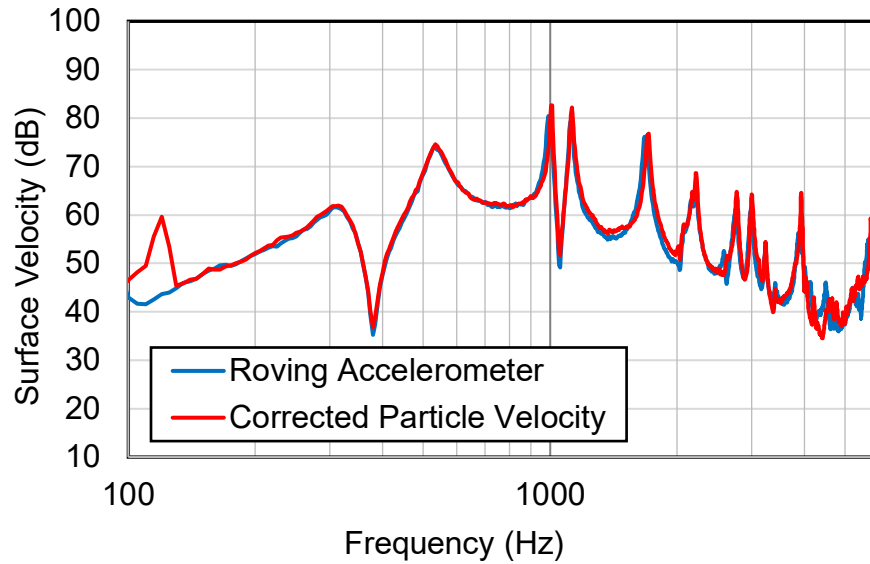

Figure 4.7 – Corrected velocity measurements for the oil pan test case from 100-6000 Hz.

4.2.4 Gas Tank Velocity Corrections

The final test case examined is the gas tank attached to the internal combustion engine. This example presents a number of challenges that are anticipated in operating machinery. First, the gas tank is close to several other source components. Secondly, the gas tank has a complicated geometry. For practical purposes, PU probe measurements cannot be made at the same distance away from the surface. Measurements were hence made by hand at approximately 1.5 cm from the surface. Finally, the gas tank is only driven at the engine harmonic frequencies and not by broadband shaker excitation. For these reasons, the gas tank test case should test the robustness of the correction approach.

The top surface of the gas tank was used for measuring the correction transfer function. It is the most exposed surface and it is also flatter than the other surfaces. Patch 2 on the top of the gas tanks was selected. The transfer function between the surface velocity measured with an accelerometer and particle velocity measured at 1.5 cm away with the PU probe was measured in one-third octave bands. No running average was performed in

51

this case. Figure 4.8 shows the correction which is relatively constant over the full frequency range from 125 to 5000 Hz.
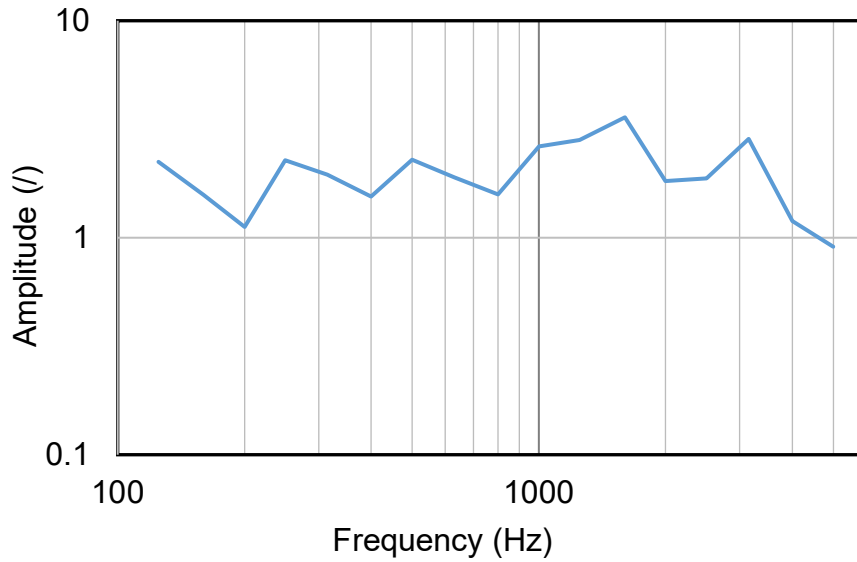
Figure 4.8 – Transfer function between particle velocity at 1.5 cm away and surface velocity at Patch 2 on the top of the gas tank. 125-5000 Hz, third-octave bands.
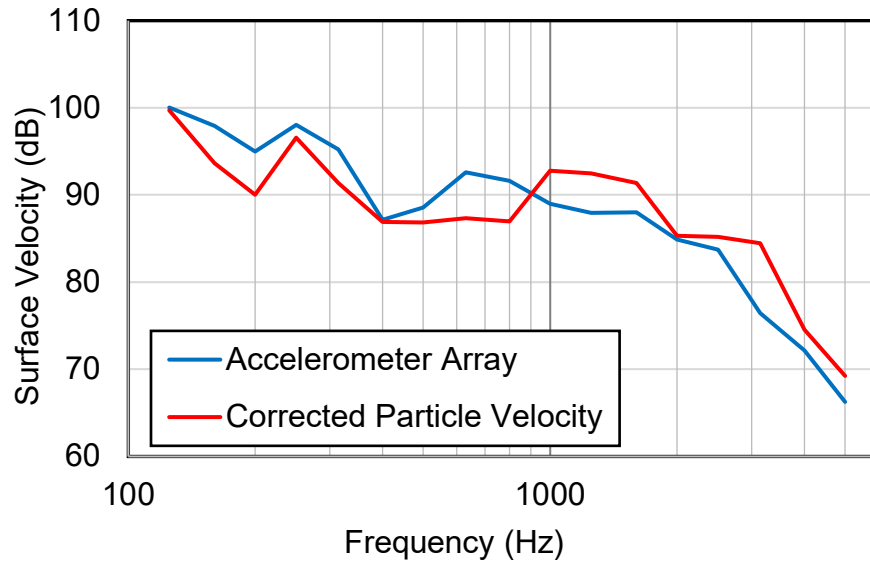
Figure 4.9 – Corrected velocity measurements for the gas tank from 100-6000 Hz.

The corrected average particle velocity is compared to direct measurement of average acceleration in Figure 4.9. Agreement is acceptable over the full frequency range of interest.

4.3 Radiation Efficiency with Surface Velocity Corrections

4.3.1 Aluminum Plate Corrected Radiation Efficiency

The radiation efficiency for the aluminum plate was recalculated using the corrected particle velocity. The sound power was measured using the PU probe in both cases. Radiation efficiency is compared in Figure 4.10 It can be observed that agreement is excellent over the entire frequency range.
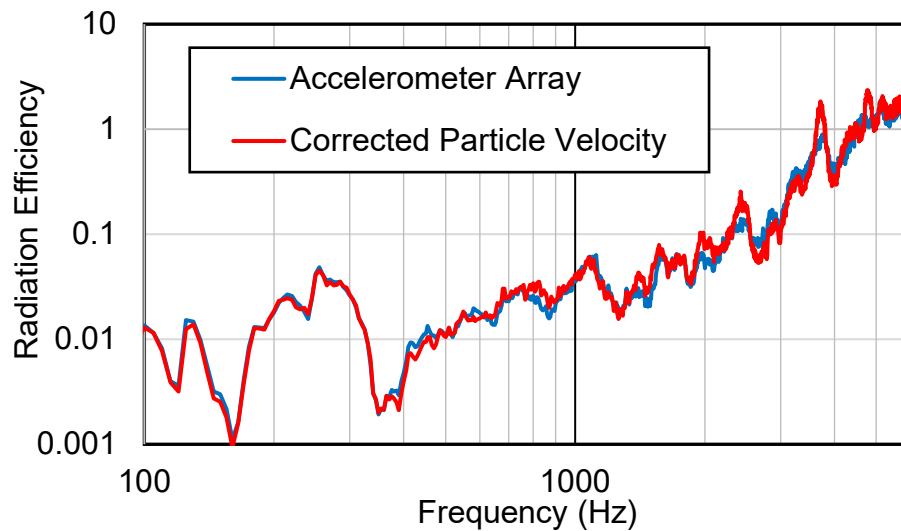
Figure 4.10 – Radiation efficiency for aluminum plate after particle velocity correction, 100-6000 Hz.

4.3.2 Stainless-Steel Plate Corrected Radiation Efficiency

The radiation efficiency was also calculated for the 1 mm stainless-steel plate using the corrected particle velocity. For both cases, the sound power was determined by scanning with the PU probe. The radiation efficiency is compared in Figure 4.11. These results are less accurate than those for the aluminum plate, but the correlation is nonetheless acceptable and will be suitable for engineering purposes.
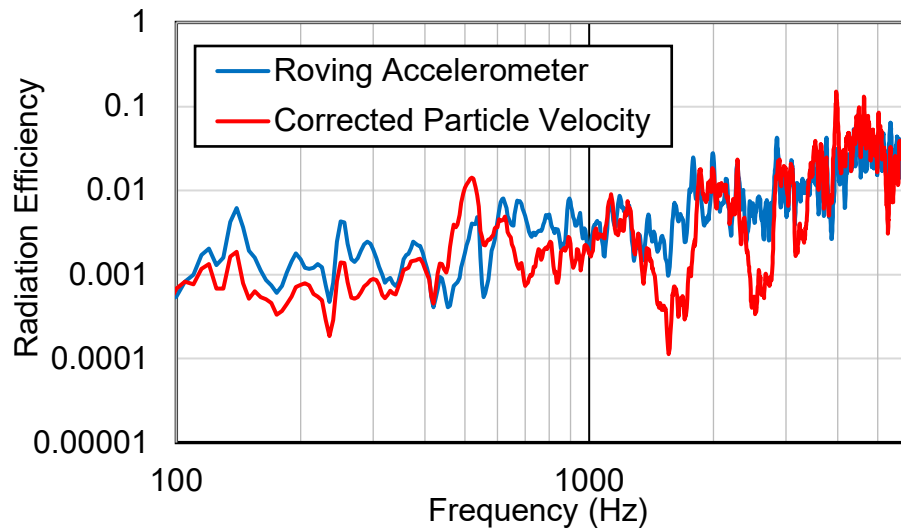
Figure 4.11 – Radiation efficiency for stainless-steel plate after particle velocity correction, 100-6000 Hz.

4.3.3 Oil Pan Corrected Radiation Efficiency

The procedure was then repeated for the oil pan. The radiation efficiencies determined using the corrected particle velocity and direct accelerometer measurements are compared in Figure 4.12. Notice that the agreement is excellent except at the higher frequencies. In this case, the results are likely better using the corrected particle velocity. This is due to the fact that surface vibration results are too low when the accelerometer is located at a node line. In addition, there is also a mass loading effect since the natural frequencies of the oil pan shift slightly when the accelerometer is roved on the plate. These results suggest that the PU probe may prove advantageous since it is a non-contact approach.

54
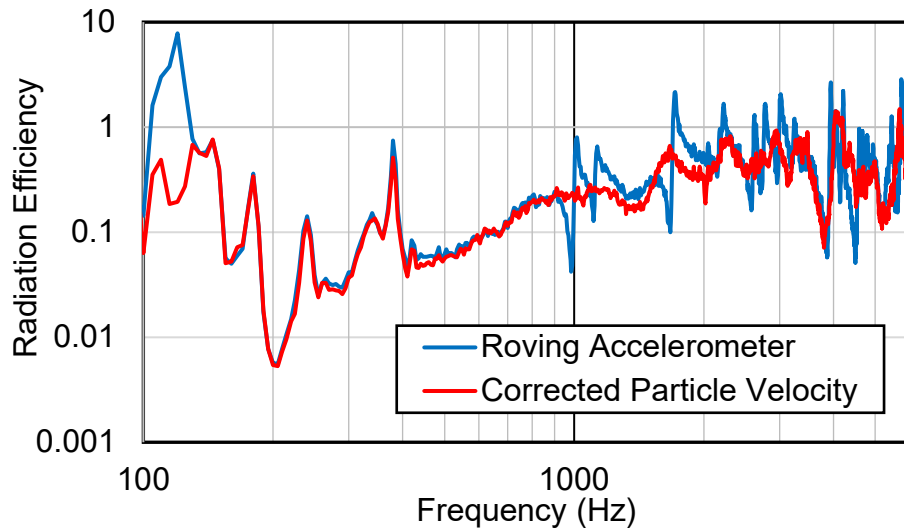
Figure 4.12 – Radiation efficiency for stainless-steel plate after particle velocity correction, 100-6000 Hz.

4.3.4 Gas Tank Corrected Radiation Efficiency

The last case considered is the gas tank attached to the internal combustion engine. The difficulties of this case were noted earlier in Section 4.2.4. Corrected particle velocity was again used to determine the radiation efficiency. Radiation efficiency is compared between corrected PU probe and direct acceleration measurement in Figure 4.13. Agreement is generally good between the two curves. As an engineering method, the PU probe measurements are certainly acceptable.

In summary, an alternate method for determination of radiation efficiency has been proven. By correcting particle velocity measurements with a single transfer function measurement, surface velocity can be accurately obtained with the PU probe. After completing a sound intensity scan with the PU probe, sound power can also be determined. Combining these two measurements and Equation 2.1, radiation efficiency can be measured accurately. This has been proven on a diverse pool of complex vibrating structures under various forcing functions. Accuracy for this method is on the order of the methods proposed in ISO-7849.
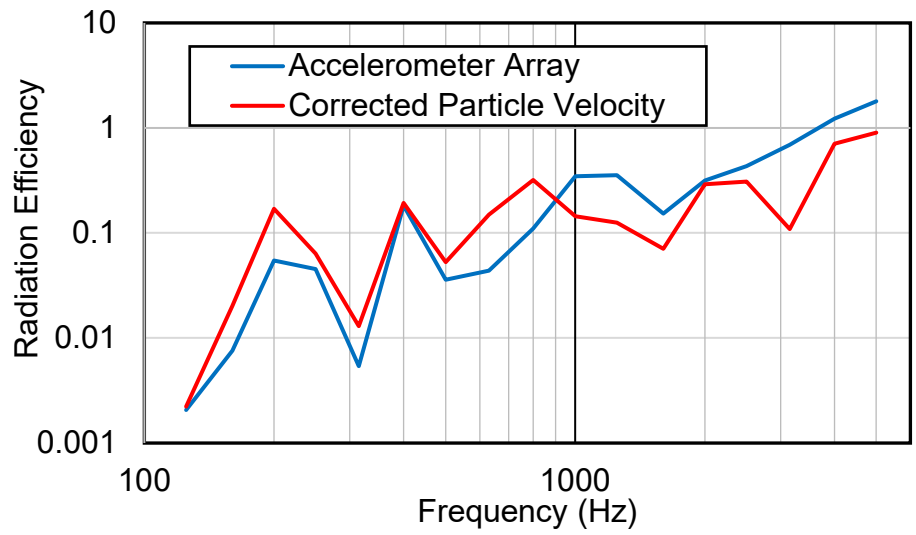
Figure 4.13 – Radiation efficiency for the gas tank after particle velocity correction, 125-5000 Hz.

CHAPTER 5 CONCLUSIONS AND FUTURE WORK

5.1 Conclusions

Acoustic radiation efficiency is defined as the radiated sound power divided by the equivalent sound power from a baffled piston. It is well known that radiation efficiency will approach or even exceed unity when the structural wavelength is on the same order as or greater than the acoustic wavelength. The structural and acoustic wavelengths are equal to one another at the coincidence frequency. This coincidence frequency can be increased by reducing the thickness of a plate or more generally by reducing the stiffness. In low stress components, the thickness can be reduced and low radiation efficiency can be taken advantage of to reduce the emitted noise.

In the research reported in this thesis, a sound pressure - particle velocity combination probe or PU probe is used to measure radiation efficiency. The suggested method appears to be a promising alternative to ISO-7849 [25]. If ISO-7849 is used, the sound power is measured using a sound intensity probe and the surface vibration is measured using accelerometers. The PU probe permits direct and simultaneous measurement of sound power and particle velocity at some distance from the vibrating surface. However, the particle velocity will not be equal to the surface vibration because the particle velocity decays with distance from the surface. Hence, it is best to measure close to the surface and correct the result to better correlate with the surface vibration.

Test cases include a 3.175 mm thick aluminum plate, 1 mm thick stainless-steel plate, a ribbed aluminum oil pan, and a two-shell composite gas tank. Based on these test cases, it was established that the sound power could be accurately measured using the PU probe and that the measured particle velocity could be corrected to correlate well with direct measurement of surface vibration. It was shown that the most straightforward correction was to measure acceleration on the surface and measure particle velocity at a set distance away. The transfer function between the two measurements can be used as the correction. By using the correction, it was shown that the radiation efficiency could be accurately determined for each case.

5.2 Future Work

The current research paves the way for additional studies. These might include additional validation of the measurement of radiation efficiency on other examples. The current test cases were all plate-like structures. The approach should be further validated for a solid component like an engine block.

Secondly, further work should be performed to establish a protocol for a scanning measurement approach. This will likely include validating a correction approach and selection of an optimal distance away from the source for measurement of particle velocity. It is desirable to select a distance so that both sound power and the estimated surface vibration can be determined with a single scan.

REFERENCES

1. ISO/TS 7849 - 1, "Acoustics — Determination of airborne sound power levels emitted by machinery using vibration measurement — Part 1: Survey method using a fixed radiation Factor", *International Organization for Standardization*, Geneva, (2009).

2. L. Cremer, M. Heckl, B. A. T. Peterson, *Structure-Borne Sound*, 3rd Edition, Springer, (2005).

3. D. A. Bies, C. H. Hansen, and C. Q. Howard, *Engineering Noise Control*, 5th Edition, CRC Press, Boca Raton, FL (2018).

4. F. G. Leppington, E. G. Broadbent and K. H. Heron, "The Acoustic Radiation Efficiency of Rectangular Panels", *Proceedings of the Royal Society of London. Series A, Mathematical and Physical Sciences*, **382**(1783), 245-271, (1982).

5. Bjorn Forssen and Malcom J. Crocker, "Estimation of acoustic velocity, surface velocity, and radiation efficiency by use of the two-microphone method", *The Journal of the Acoustical Society of America*, **73**(3), 1047-1053, (1983).

6. C. H. Hansen and D. A. Bies, "Near Field Determination of the Complex Radiation Efficiency and Acoustic Intensity Distribution for a Resonantly Vibrating Surface", *Journal of Sound and Vibration*, **62**(1), 93-110, (1979).

7. John L. Davy et al, "Comparison of theoretical predictions of radiation efficiency with experimental measurements", *Proceedings of the 22nd International Congress on Sound and Vibration*, (2015).

8. H. P. Wallin et al, *Sound and Vibration*, KTH, Stockholm, (1999).

9. Stephen A. Hambric, Shung H. Sung, Donald J. Nefske, *Engineering Vibroacoustic Analysis: Methods and Applications*, 1st Edition, Wiley, West Sussex, United Kingdom, (2016).

10. David A. Bies and Colin H. Hansen, *Engineering Noise Control*, 4th Edition, CRC Press, New York, New York (2009).

11. M. Long, *Architectural Acoustics*, 2nd Edition, Academic Press, Waltham, MA, (2014).

12. Giancarlo Genta, *Vibration Dynamics and Control*, Springer, (2009).

13. Mark F. Jacobsen, Rajendra Singh and Fred B. Oswald, "Acoustic Radiation Efficiency Models of a Simple Gearbox", (Army Research Laboratory Technical

Report 1111), *Prepared for the Seventh International Power Transmission and Gearing Conference*, (1996).

14. Jianxing Zhou, Geng Liu, and Shangjun Ma, "Noise radiation Analysis of Structural-Acousitc Coupling System of a Gear Box", *Applied Mechanics and Materials*, **37-38**, 718-722, (2010)

15. David Allen Hamilton, *A Comparison of the Boundary Element and Rayleigh Integral Methods for Calculating Noise from Vibrating Bodies*, University of Kentucky, (1996).

16. J. C. S. Lai and M. A. Burgess, "Radiation efficiency of acoustic guitars", *The Journal of the Acoustical Society of America*, **88**(3), 1222-1227, (1990)

17. Z. G. Zhao, Q. B. Huang and Z. He, "Calculation of sound radiant efficiency and sound radiant modes of arbitrary shape structures by BEM and general eigenvalue decomposition", *Applied Acoustics*, **69**, 796-803, (2008)

18. Lukasz J. Nowak and Tomasz G. Zielinski, "Determination of the Free-Field Acoustic Radiation Characteristics of the Vibrating Plate Structures With Arbitrary Boundary Conditions", *Journal of Vibration and Acoustics*, **137**(5), (2015)

19. ISO/TS 7849-2, "Acoustics — Determination of airborne sound power levels emitted by machinery using vibration measurement — Part 2: Engineering method including determination of the adequate radiation factor", *International Organization for Standardization*, Geneva, (2009).

20. Thomas D. Rossing, *Handbook of Acoustics*, Springer, (2007).

21. K Beissner, "On the plane-wave approximation of acoustic intensity", *The Journal of the Acoustical Society of America*, **71**(6), 1406-1411, (1982)

22. Lawrence E. Kinsler et al, *Fundamentals of Acoustics*, 4th Edition, Wiley, (2000).

23. Peter Juhl and Finn Jacobsen, "A note on measurement of sound pressure with intensity probes", *The Journal of the Acoustical Society of America*, **116**(3), 1614-1620, (2004)

24. Mei Q. Wu and Malcolm J. Corcker, "The properties of the estimation error of sound power measurement using sound intensity techniques", *The Journal of the Acoustical Society of America*, **85**(3), 1182-1190, (1989).

25. ISO-9614-2, "Acoustics — Determination of sound power levels of noise sources using sound intensity— Part 2:Measurement by scanning", *International Organization for Standardization*, Geneva, (1996).

26. F. Jacobsen, "Random Errors in Sound Power Determination Based on Intensity Measurement", *Journal of Sound and Vibration*, **131**(3), 475-487, (1989)

27. Finn Jacobsen, "An Overview of the Sources of Error in Sound Power Determination Using the Intensity Technique", *Applied Acoustics*, **50**(2), 155-166, (1997)

28. Finn Jacobsen, "On the uncertainty in measurement of sound power using sound intensity", *Noise Control Engineering*, **55**(1), (2007)

29. Hans-Elias de Bree et al, "The μ-flown: a novel device for measuring acoustic flows", *Sensors and Actuators A: Physical*, **54**(1-3), 552-557 (1996).

30. Hans-Elias de Bree, "The Microflown, a New Particle Velocity Sensor", *Sound and Vibration Journal*, **39**(2), 8, (2005).

31. Hans-Elias de Bree et al, "The Sound Pressure Microflown A novel Way of Transducing Sound Pressure", *MME*, (2000).

32. Hans-Eliad de Bree, W. F. Druyvesteyn and Miko Elwenspoek, "Realisation and Calibration of a Novel Half Inch P-U Sound Intensity Probe", *106th Audio Engineering Society Convention*, Munich, Germany, (1999).

33. R. Raangs, W. F. Druyvesteyn and H. E. de Bree, "A low cost Intensity Probe", *110th Audio Engineering Society Convention*, Amsterdam, The Netherlands, (2001).

34. J. van Honschoten et al, "Application of a microflown as a low-cost level sensor", *Journal of Micromechanics and Microengineering*, **10**, 250-253, (2000).

35. Hans-Elias de Bree, Ron Raangs, and Erik Druyvesteyn, "Sound intensity measurements with the Microflown sensor", *33rd International Congress and Exposition on Noise Control Engineering*, Praque, Czech Republic, (2004).

36. J. W. van Honschoten et al, "Analytic model of a two-wire thermal sensor for flow and sound measurements", *Journal of Micromechanics and Microengineering*, **14**, 1468-1477, (2004).

37. W. F. Druyvesteyn, "A new sound intensity probe; (Comparison to the "pair of pressure microphone" intensity probe)", *Journal of Audio Engineering Society*, **48**(1-2), (2000).

38. V. B. Svetovoy and I. A. Winter, "Model of the μ-flown microphone", *Sensors and Actuators*, **86**, 171-181, (2000).

39. Joost W. van Honschoten et al, "Optimization of a Thermal Flow Sensor for Acoustic Particle Velocity Measurements", *Journal of Microelectromechanical Systems*, **14**(3), (2005).

40. F. J. M. van der Eerden, H-E. de Bree, H. Tijdeman, "Experiments with a new acoustic particle velocity sensor in an impedance tube", *Sensors and Actuators A69*,(1998).

41. Hans-Elias de Bree and Miko Elwenspoek, "The Microflown, from die to product", *Proceedings of the 13th European Conference on solid state transducers*, 459-460, (1999).

42. Finn Jacobsen, and Virginie Jaud. "A note on the calibration of pressure-velocity sound intensity probes", *The Journal of the Acoustical Society of America*, **120**(2), 830-837 (2006).

43. D. Stanzial and D. Bonsi, "Calibration of the p-v Microflown® probe and some considerations on the physical nature of sound impedance", *5th European Conference on Noise Control*, Naples, Italy, (2003).

44. Hans-Elias de Bree and Miko Elwenspoek, "Sound Intensity Probes Based on Microflown Technology", *ASA Berlin*, (1999).

45. H-E. de Bree et al, "The Very Near Field Theory; Simulation and Measurements of Sound Pressure and Particle Velocity in the Ver Near Field", *11th International Congress on Sound and Vibration*, St. Petersburg, Russia, (2004).

46. Daniel Fernandez Comesaña, Fan Yang and Emiel Tijs, "Influence of background noise on non-contact vibration using particle velocity sensors", *43rd International Congress on Noise Control Engineering*, Melbourne, Australia, (2014).

47. C. Pezerat et al, "Identification of vibration excitations from acoustic measurements using nearfield acoustic holography and the force analysis technique." *Journal of Sound and Vibration*, **326**, 540-556, (2009).

48. Daniel Fernandez Comesaña, Hans-Elias de Bree and Jelmer Wind, "Measuring Operational Deflection Shapes with a Scanning P-U Probe", *19th International Congress on Sound and Vibration*, Vilnius, Lithuania, (2012).

49. K. Beissner, "Acoustic radiation pressure in the near field", *Journal of Sound and Vibration*, **93**(54), 537-548, (1984).

50. Daniel Fernandez Comesaña, Bilen Oytun Peksel and Hans-Elias de Bree, "Expanding the Sound Power Measurement Criteria for Sound Intensity P-U Probes", *21st International Congress on Sound and Vibration*, Beijing, China, (2014).

51. Finn Jacobsen and Hans-Elias de Bree, " A Comparison of P-P and P-U Sound Intensity Measurement Systems", *11th International Congress on Sound and Vibration*, St. Petersburg, Russia, (2004).

52. Finn Jacobsen, and H-E de Bree, "Measurement of sound intensity: p-u probes versus p-p probes", *Proceedings of NOVEM 2005*, (2005).

53. Finn Jacobsen, and Hans-Elias de Bree, "A comparison of two different sound intensity measurement principles", *The Journal of the Acoustical Society of America*, **118**(3), 1510-1517 (2005).

54. Daniel Fernandez Comesaña and Emiel Tijs, "Assessing Engine Noise Using Particle Velocity Sensors", *Sound and Vibration*, **50**(9), 10-14, (2016).

55. Lin Geng et al, "Reconstruction of instantaneous surface normal velocity of a vibrating structure using interpolated time-domain equivalent source method", *Mechanical Systems and Signal Processing*, **107**, 1-11, (2018).

56. Efren Fernandez-Grande, Finn Jacobsen, and Quentin Leclère, "Sound field separation with sound pressure and particle velocity measurements", *The Journal of the Acoustical Society of America*, **132**(6), 3818-3825, (2012).

57. Hans-Elias de Bree and Jelmer W. Wind, "The acoustic vector sensor: a versatile battlefield acoustics sensor", *Proceedings of SPIE Defense, Security, and Sensing 2011*, **8047**, Orlando, Florida, (2011).

58. Davide Bonsi and Domenico Stanzial, "Use of the Microflown® Intensity Probe for evaluating the Influence of the Environment on the Power of an Acoustic Source", *18th International Congress on Acoustics*, Kyoto, Japan, (2004).

<h1 style="text-align: center;">VITA</h1>

<h1 style="text-align: center;">STEVEN CONNER CAMPBELL</h1>

PLACE OF BIRTH

Corbin, Kentucky

EDUCATION

Eastern Kentucky University
Bachelor of Science in Physics with Honors (July 2016)

PROFESSIONAL POSITIONS

Lockheed Martin (Production Engineer Planner)
Lexington, Kentucky (September 2018-April 2019)

University of Kentucky ME Dept. (Graduate Student/Research Engineer)
Lexington, Kentucky (March 2017-September 2018)

Briggs and Stratton (NVH Intern)
Milwaukee, Wisconsin (May 2017- August 2017)

Tribo Flow Separations (Research Engineer)
Lexington, Kentucky (August 2016- March 2017)

Aisin Automotive Casting Tennessee (Quality Engineer Intern)
Clinton, Tennessee (June 2016- August 2016)

CONFERENCE PROCEEDINGS

Steven Campbell, D. W. Herrin, Brett Birshbach, and Pat Crowley, "Notes on Measurement of Radiation Efficiency", *Inter-Noise 2018 Conference*, Chicago, Illinois, August 26-29, 2018.

D. W. Herrin, Gong Cheng, Steven C. Campbell, and J. M. Stencel, "Noise reduction on a jumbo drill using panel contribution analysis and scale modeling", *Inter-Noise 2017 Conference*, Hong Kong, China, August 27-30, 2017.